

Close Encounters of Wide Binaries Induced by the Galactic Tide: Implications for Stellar Mergers and Gravitational-Wave Sources

JAKOB STEGMANN ¹, ALEJANDRO VIGNA-GÓMEZ ¹, ANTTI RANTALA ¹, TOM WAGG ², LORENZ ZWICK ³,
MATHIEU RENZO ⁴, LIEKE A. C. VAN SON ⁵, SELMA E. DE MINK ^{1,6} AND SIMON D. M. WHITE ¹

¹*Max-Planck-Institut für Astrophysik, Karl-Schwarzschild-Straße 1, 85741 Garching bei München, Germany*

²*Department of Astronomy, University of Washington, Seattle, WA 98195, USA*

³*Niels Bohr International Academy, Niels Bohr Institute, Blegdamsvej 17, 2100 København, Denmark*

⁴*Steward Observatory, University of Arizona, 933 N Cherry Avenue, Tucson, AZ 85721, USA*

⁵*Center for Computational Astrophysics, Flatiron Institute, New York, NY 10010, USA*

⁶*Ludwig-Maximilians-Universität München, Geschwister-Scholl-Platz 1, 80539 München, Germany*

ABSTRACT

A substantial fraction of stars can be found in wide binaries with projected separations between $\sim 10^2$ and 10^5 AU. In the standard lore of binary physics, these would evolve as effectively single stars that remotely orbit one another on stationary Keplerian ellipses. However, embedded in their Galactic environment their low binding energy makes them exceptionally prone to perturbations from the gravitational potential of the Milky Way and encounters with passing stars. Employing a fully relativistic N -body integration scheme, we study the impact of these perturbations on the orbital evolution of wide binaries along their trajectory through the Milky Way. Our analysis reveals that the torques exerted by the Galaxy can cause large-amplitude oscillations of the binary eccentricity to $1 - e \lesssim 10^{-8}$. As a consequence, the wide binary members pass close to each other at periastris, which, depending on the type of binary, potentially leads to a mass transfer or collision of stars or to an inspiral and subsequent merger of compact remnants due to gravitational-wave radiation. Based on a simulation of 10^5 wide binaries across the Galactic field, we find that this mechanism could significantly contribute to the rate of stellar collisions and binary black hole mergers as inferred from observations of Luminous Red Novae and gravitational-wave events by LIGO/Virgo/Kagra. We conclude that the dynamics of wide binaries, despite their large mean separation, can give rise to extreme interactions between stars and compact remnants.

1. INTRODUCTION

In recent years, unprecedented astrometric data obtained with the *Gaia* spacecraft have revealed numerous wide stellar binaries with projected separations between $\sim 10^2$ and 10^5 AU (Andrews et al. 2017; Oelkers et al. 2017; El-Badry & Rix 2018; Jiménez-Esteban et al. 2019; Hartman & Lépine 2020; Tian et al. 2020; Hwang et al. 2021; El-Badry et al. 2021; El-Badry 2024). For instance, El-Badry & Rix (2018) identified $\sim 5.5 \times 10^4$ wide main-sequence and white dwarf binaries in the *Gaia* DR2 sample within a distance $d < 200$ pc to the Sun. Given a local total stellar number density of $n_\star \approx 0.1/\text{pc}^3$ this implies that at least several per cent

of all stars in the solar neighborhood and possibly within the Galaxy must be part of a wide binary. Indeed, estimates from the *Gaia* Early Data Release 3 indicate that the wide binary fraction of nearby FGK stars is as large as 10 – 12 % (Gaia Collaboration et al. 2021).

In the standard lore of binary physics, wide binaries (simply denoted as “binaries”, hereafter) are thought to evolve as non-interacting, effectively single stars (e.g., Sana et al. 2012). However, this is only true as long as the binaries are assumed to be in isolation. In reality, they are embedded in a galactic environment in which their low binding energy makes them susceptible to perturbations from the gravitational potential of their host galaxy and encounters with passing stars and giant molecular clouds. The effect of these perturbations has been studied in a wide range of different contexts, e.g., to constrain the existence of a distant companion to our Sun (Antonov & Latyshev 1972; Whitmire & Jackson

1984; Davis et al. 1984; Hut 1984; Weinberg et al. 1987; Melott & Bambach 2010; Matese & Whitmire 2011; Luhman 2014), to probe the nature of dark matter (Yoo et al. 2004; Quinn et al. 2009; Monroy-Rodríguez & Allen 2014; Peñarrubia et al. 2016) and gravity (Pitordis & Sutherland 2019; Banik et al. 2023), to explore the stability of binaries with a distant tertiary companion (Kaib et al. 2013; Correa-Otto & Gil-Hutton 2017; Antonini et al. 2017; Michaely & Perets 2020; Grishin & Perets 2022), and to form colliding stars (Kaib & Raymond 2014) and compact object mergers (Michaely & Perets 2019, 2020; Raveh et al. 2022).

From a dynamical point of view, it is understood that the Galactic perturbations could generally lead to two different extreme outcomes: they may either dissolve the wide binary (e.g., Weinberg et al. 1987; Jiang & Tremaine 2010; Correa-Otto & Gil-Hutton 2017) or they torque it to an eccentric orbit on which the two binary members pass close to each other at periastris (e.g., Heisler & Tremaine 1986; Collins & Sari 2008; Kaib & Raymond 2014; Correa-Otto et al. 2017; Modak & Hamilton 2023; Hamilton & Modak 2023). These findings were largely made using one or more of the following assumptions:

1. The Galactic potential is averaged over the long orbital period of the binary (also known as secular approximation).
2. The gravitational perturbation from the Galactic potential is approximated by the leading-order contribution of an expansion about the binary centre of mass (barycentre).
3. Focusing on the dynamics of wide binaries in the solar neighbourhood, the perturbation from the Galactic potential is evolved along the (circular) trajectory of the Sun at a Galactocentric radius $\rho \approx 8$ kpc from the centre of the Milky Way.

However, studies of binaries orbiting in other gravitational potentials let us wonder if these assumptions lead to an underestimation of the perturbative effect of the Galactic potential on wide binaries. For instance, Hamilton & Rafikov (2019a,b, 2021) and Bub & Petrovich (2020) studied the evolution of binaries orbiting inside the smooth potential of a star cluster and found that resonant behaviour can excite their eccentricity to near-unity ($e \rightarrow 1$). Similarly, the eccentricity of binaries moving inside the Keplerian potential of a distant tertiary companion (i.e., those that form a hierarchical triple) can undergo a long-term growth to near-unity through the so-called eccentric von Zeipel-Kozai-Lidov effect (Naoz 2016). For either case, it was shown that

the external potentials exert a torque on the binaries which could remove nearly all their orbital angular momentum. Depending on the type of binary this could cause a stellar collision (Katz & Dong 2012; Kushnir et al. 2013; Toonen et al. 2018, 2020; Stegmann et al. 2022b) or a gravitational-wave capture (Antonini et al. 2014, 2017; Rodríguez & Antonini 2018) at close periastris passage.

In this regard, it would be surprising if the potential of a galaxy acted differently than the aforementioned examples. Indeed, if we consider an example stellar-mass binary (total mass $m = 1 M_\odot$) moving on circular trajectory at a Galactocentric radius $\rho = 5$ kpc on the Galactic plane and treat the Milky Way as a tertiary point mass equal to the enclosed mass $M(\rho)$ we find that the latter perturbs the binary on a characteristic (von Zeipel-Kozai-Lidov) timescale (Antonini 2015)

$$t_{\text{ZKL}} = 9.0 \text{ Gyr} \left(\frac{5.9 \times 10^{10} M_\odot}{M(\rho)} \right) \left(\frac{m}{M_\odot} \right)^{1/2} \times \left(\frac{\rho}{5 \text{ kpc}} \right)^3 \left(\frac{5 \times 10^3 \text{ AU}}{a} \right)^{3/2}. \quad (1)$$

While this toy model (Chebotarev 1966) indicates that the tertiary “Galaxy companion” could induce large-amplitude oscillations of the binary eccentricity within a Hubble time for wide semi-major axes $a \gtrsim \mathcal{O}(10^3)$ AU, it cannot serve as more than a simple back-of-the-envelope estimate to motivate this work.

Here, we develop a numerical method to evolve the relativistic dynamics of binaries following the mutual gravitational interaction between the two members, the force exerted by the Galaxy in which they orbit, and the effect of encountering stars. Crucially, to accurately evolve binaries which are torqued to a very eccentric orbit we employ a direct N -body approach rather than any secular code that derives from a time- (e.g., orbit-) averaged Hamiltonian. While the secular approximation is oftentimes used to efficiently evolve a large number of, e.g., hierarchical triples (e.g., Naoz et al. 2013; Rodríguez & Antonini 2018; Liu & Lai 2019; Stegmann et al. 2022a) and binaries inside clusters (e.g., Hamilton & Rafikov 2019c; Bub & Petrovich 2020) it has been shown that it tends to underestimate the maximum possible eccentricity because it washes out any short-term variability of the torque exerted by the perturbing potential (Antonini et al. 2014, 2017; Hamilton & Rafikov 2024). These shortcomings are circumvented by using a full direct N -body integration scheme which, in our case, adds little computational costs because of the low number of particles ($N = 2$).

The aim of this work is to use this integrator which relies on none of the aforementioned assumptions (1–3) in

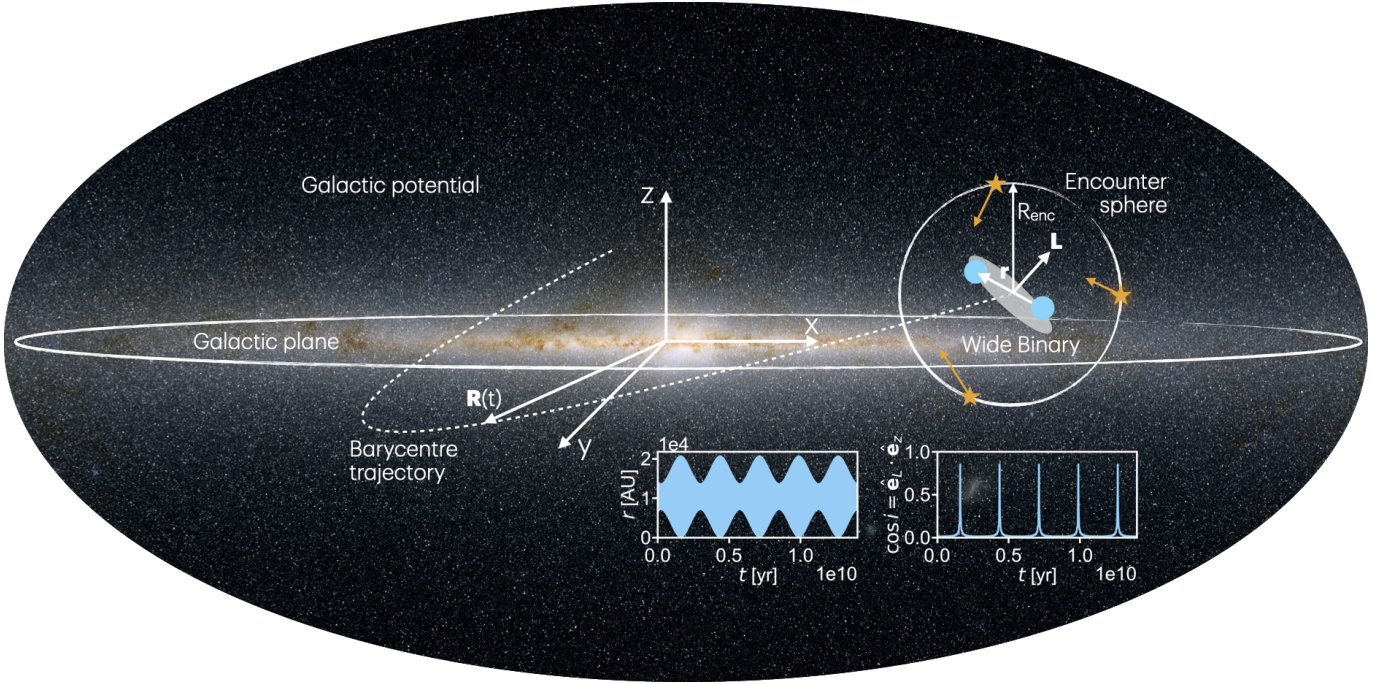


Figure 1. Schematic overview of the problem considered in this work. We study the dynamical evolution of wide binaries along their barycentre trajectory $\mathbf{R} = \mathbf{R}(t)$ through the Galaxy (dashed curve), denoting its projection onto the Galactic plane as $\boldsymbol{\rho} = \boldsymbol{\rho}(t)$. We consider one model in which the wide binaries are solely perturbed by the axisymmetric Galactic potential Φ and another one where we additionally include the impulsive effect of ambient stars impinging on the encounter sphere (solid circle) with radius R_{enc} from the binary barycentre. The main effect of the Galactic perturbations is to torque the binary orbital angular momentum \mathbf{L} leading to large-amplitude oscillations of the binary eccentricity e , and hence its peri- and apoapsis $r = a(1 \mp e)$, and the relative orientation $\cos(i) = \hat{\mathbf{e}}_L \cdot \hat{\mathbf{e}}_z$ of the orbital plane w.r.t. the Galactic frame (insets). The dimensions are not drawn to scale. The Atlas Image of the Milky Way in the near infrared used as a background is courtesy of 2MASS/UMass/IPAC-Caltech/NASA/NSF.

order to systematically and accurately study the dynamical evolution of wide binaries throughout the Galaxy. The primary focus is to understand their dynamical evolution treating the binary members as point masses. We highlight potential implications for wide binary *stars* and wide binary *compact objects*, where stellar tides or natal kicks also may play a role, but defer a thorough investigation to a follow-up study.

This paper is organised as follows. In Sec. 2, we present our method to evolve the wide binaries. In Sec. 2.4, we describe how we initiate a population of wide binaries whose dynamical evolution we simulate along their trajectory through the host galaxy. In Sec. 3, we present the results of their numerical integration. Finally, our findings are summarised and discussed in Sec. 5.

2. METHODS

2.1. Equations of motion and numerical integration

We study the dynamical evolution of wide binaries as they move through the smooth gravitational potential Φ of their host Galaxy. Denoting the masses, positions, and velocities of the two binary members as m_i , \mathbf{r}_i , and

\mathbf{v}_i ($i = 1, 2$), respectively, the equations of motion can be written as¹

$$\frac{d\mathbf{r}_i}{dt} = \mathbf{v}_i, \quad (2)$$

$$\frac{d\mathbf{v}_i}{dt} = \mathbf{a}_i + \mathbf{g}_i + \mathbf{f}_i, \quad (3)$$

where

$$\mathbf{a}_i = Gm_j \frac{\mathbf{r}_j - \mathbf{r}_i}{\|\mathbf{r}_j - \mathbf{r}_i\|^3} \quad (i \neq j) \quad (4)$$

is the Newtonian acceleration due to the binary companion and $\mathbf{f}_i = -\nabla\Phi|_{\mathbf{r}_i}$ is the acceleration due to the external Galactic potential. Relativistic corrections to the internal binary motion are captured by the velocity-dependent post-Newtonian accelerations $\mathbf{g}_i = \mathbf{g}_i(\mathbf{r}_j - \mathbf{r}_i, \mathbf{v}_j - \mathbf{v}_i)$ with $i \neq j$. We can characterise the orbit of the binary in terms of its angular momentum vector \mathbf{L}

¹ Throughout this work, the magnitude, unit vector, and time derivative of some vector \mathbf{V} are written as $V = \|\mathbf{V}\|$, $\hat{\mathbf{e}}_V = \mathbf{V}/V$, and $\dot{\mathbf{V}} = d\mathbf{V}/dt$, respectively. G refers to the gravitational constant.

and eccentricity vector \mathbf{e} which are

$$\mathbf{L} = \mu \mathbf{r} \times \mathbf{v}, \quad (5)$$

$$\mathbf{e} = \frac{\mathbf{v} \times (\mathbf{r} \times \mathbf{v})}{Gm} - \frac{\mathbf{r}}{r}, \quad (6)$$

where $\mathbf{r} = \mathbf{r}_2 - \mathbf{r}_1$ and $\mathbf{v} = \mathbf{v}_2 - \mathbf{v}_1$ are the relative separation and velocity vectors, and $m = m_1 + m_2$ and $\mu = m_1 m_2 / m$ are the total and reduced mass of the binary, respectively. They have magnitudes $L = \mu \sqrt{Gma(1-e^2)}$ and $\|\mathbf{e}\| = e$, where a and e are the semi-major axis and eccentricity of the orbit, respectively. Erecting a frame in which the Galaxy is centred at $x = y = z = 0$ and defining the Galactic plane as $z = 0$, we denote the position of the binary barycentre as $\mathbf{R} = (R_x, R_y, R_z)^T$ and its projection onto the Galactic plane as $\boldsymbol{\rho} = (R_x, R_y, 0)^T$. Fig. 1 shows a schematic overview of our considered geometry.

In the absence of any perturbative force ($\mathbf{f}_i = \mathbf{g}_i = 0$) the equations of motion (2) – (3) reduce to that of a Keplerian orbit which preserves \mathbf{L} and \mathbf{e} . As we will see, however, the forces exerted by the Galactic potential and stellar encounters (Sec. 2.3) can put the binary members on a nearly radial orbit ($e \rightarrow 1$) on which they pass each other at an extremely close pericentre distance $r = a(1-e) \ll a$ despite their wide semi-major axis. To accurately recover their evolution it is necessary that we also include post-Newtonian corrections \mathbf{g}_i to Eq. (3) which we do to 3.5 order (Mora & Will 2004).

To evolve the equations of motion (2) and (3) we use the publicly available direct N -body integrator **MSTAR** (Rantala et al. 2020; Mannerkoski et al. 2023) which is based on an algorithmically regularized integration technique (e.g., Mikkola & Tanikawa 1999; Preto & Tremaine 1999; Mikkola & Merritt 2008; Hellström & Mikkola 2010; Trani & Spera 2023). The time-transformed versions of the equations of motion (2) and (3) that **MSTAR** integrates are Eqs. (7) and (8) in Rantala et al. (2020). The Gragg-Bulirsch-Stoer (GBS) extrapolation technique (Gragg 1965; Bulirsch & Stoer 1966) is used to achieve an extremely high integration accuracy. Briefly, in the GBS method a longer timestep Δt is subdivided into n substeps with lengths $\Delta t/n$ and integrated with a suitable numerical integrator, in our case the leapfrog. As n is increased, the results will in general converge towards the exact solution of the equations of motion over Δt . Finally, the results are extrapolated to $n \rightarrow \infty$ using a polynomial or rational function extrapolation. We use a Gragg-Bulirsch-Stoer error tolerance parameter of $\eta_{\text{GBS}} = 10^{-12}$. The **MSTAR** endtime iteration tolerance parameter is set to $\eta_t = 10^{-6}$. For more details of **MSTAR** and the algorithmic regularization see Rantala et al. (2020) and the appendices of Rantala

et al. (2017). In particular, by accounting for the post-Newtonian corrections, **MSTAR** has the capability to follow the inspiral and the subsequent merger of the binary members due to the emission of gravitational waves until they come as close as twelve combined Schwarzschild radii.

2.2. Gravitational potential of the Galaxy

We have modified **MSTAR** to also include the ability to follow the position of the binary barycentre and the relative acceleration due to the external Galactic potential as in Eqs. (2) and (3). Here, we adopt an axisymmetric mass-model for the Milky Way from Price-Whelan (2017) consisting of a spherical nucleus and bulge, a spherical NFW dark matter halo, and an exponential disk. The numerical values for the parameters of all components of the potential which are explicated in the following are adopted from the model of Price-Whelan et al. (2024) which is based on the kinematic Milky Way analysis of Eilers et al. (2019) and Darragh-Ford et al. (2023). Specifically, the potentials of the nucleus and the bulge as a function of the binary member positions \mathbf{r}_i are modelled with a Hernquist (1990) profile

$$\Phi_{\text{Hernquist}}(\mathbf{r}_i) = -\frac{GM}{r_i + c}, \quad (7)$$

where for the nucleus we use $M = 1.814 \times 10^9 M_\odot$ and $c = 6.889 \times 10^{-2}$ kpc and for the bulge $M = 5.0 \times 10^9 M_\odot$ and $c = 1.0$ kpc. The potential of the NFW dark matter halo is given by (Navarro et al. 1996)

$$\Phi_{\text{NFW}}(\mathbf{r}_i) = -\frac{GM \ln(1 + r_i/r_s)}{r_s \frac{r_i}{r_s}}, \quad (8)$$

where $M = 5.542 \times 10^{11} M_\odot$ and $r_s = 15.626$ kpc. The stellar disk is constructed from a sum of three Miyamoto & Nagai (1975) disk potentials which models the thin and thick disk component of the Milky Way (Smith et al. 2015)

$$\Phi_{\text{Miyamoto}}(\mathbf{r}_i) = -\frac{GM}{\sqrt{x_i^2 + y_i^2 + (a + \sqrt{z_i^2 + b^2})^2}}, \quad (9)$$

where x_i , y_i , and z_i are the Cartesian components of the binary member positions, $M = 7.872 \times 10^9 M_\odot$, $a = 1.526$ kpc, and $b = 0.207$ kpc for the first instance of the potential, $M = -2.756 \times 10^{11} M_\odot$, $a = 6.783$ kpc, and $b = 0.207$ kpc for the second, and $M = 3.206 \times 10^{11} M_\odot$, $a = 5.895$ kpc, and $b = 0.207$ kpc for the third.

The total potential of our axisymmetric Milky Way model is then given by the sum of all components described by Eqs. (7) – (9). For the purpose of this work, we are ignoring more complex non-axisymmetric

features of our Galaxy such as its bar, spiral arms, and molecular cloud structure and neglecting any time-evolution of the potential. We discuss potential implications of these simplifications in Sec. 5.

2.3. Stellar encounters

In addition to the force caused by the smooth potential of the Galaxy, a wide binary experiences gravitational perturbations from encounters with passing stars. Assuming that the binary moves through a locally homogeneous and isotropic sea of stellar perturbers the rate of encounters within a distance R_{enc} to its barycentre can be written as (Hamers et al. 2021)

$$\Gamma_{\text{enc}} \approx 2\sqrt{2\pi}R_{\text{enc}}^2\sigma_{\star}n_{\star} \approx \frac{60.2}{\text{Gyr}} \left(\frac{R_{\text{enc}}}{10^4 \text{ AU}} \right)^2 \left(\frac{\sigma_{\star}}{50 \text{ km s}^{-1}} \right) \left(\frac{n_{\star}}{0.1/\text{pc}^3} \right), \quad (10)$$

where σ_{\star} and n_{\star} are the relative velocity dispersion and number density of the perturbers, respectively (Flynn et al. 2006). Eq. (10) shows that the rate of encounters quickly grows if we consider distances R_{enc} much larger than the typical relative separation of the wide binaries and modelling each of those would become computationally expensive. Fortunately, the effect on wide binaries is by far dominated by encounters which are “penetrative”, “weak”, and “impulsive” (Hamilton & Modak 2023). This means that the perturbation from the few stars which get as close as $\sim a$ to the binary (so-called “penetrative” encounters) is much stronger than the cumulative effect of the many more distant encounters, most encounters are harmless, meaning that they unlikely disrupt the binary (“weak”), and that the stellar perturbers encounter the binary on a timescale much shorter than its orbital period $T = 2\pi\sqrt{a^3/Gm}$ (“impulsive”) which is due to the fact that the typical velocity dispersion σ_{\star} of ambient stars is much larger than the orbital velocity of the binary

$$v_{\text{orb}} = 0.9 \text{ km s}^{-1} \left(\frac{m}{M_{\odot}} \right)^{1/2} \left(\frac{a}{10^3 \text{ AU}} \right)^{-1/2}. \quad (11)$$

This allows us to ignore any encounter at a distance $R_{\text{enc}} \gg a$ and to only consider close encounters which in the impulsive approximation impart an instantaneous velocity kick to the two stars of the binary.

The effect of those encounters is implemented as following. After each successful internal integration step Δt of **MSTAR** we sample a number of encounters within Δt . We do so by drawing a random number k of encounters from a Poisson distribution with mean $\lambda = \Gamma_{\text{enc}}\Delta t$. The number density n_{\star} that determines Γ_{enc} is calculated from the current position of the binary within

the Galactic disk, assuming a single perturber mass $m_p = 1 M_{\odot}$. Furthermore, we use $\sigma_{\star} = 50 \text{ km s}^{-1}$ and only consider encounters within $R_{\text{enc}} = 100r$ where r is the current relative separation of the binary.

Each of the k encounters imparts an instantaneous velocity kick to both members of the binary which is computed following Hamers & Tremaine (2017) and Hamers et al. (2021) as summarised below.

1. In an inertial frame centred at the binary barycentre, we sample a random perturber position \mathbf{R}_{enc} at a distance R_{enc} from the binary barycentre. We give the stellar perturber a random relative velocity \mathbf{V}_{enc} impinging on the encounter sphere, which is drawn from a distribution $P(\mathbf{V}_{\text{enc}}) \propto \exp(-V_p^2/2\sigma_{\star}^2)H(-\mathbf{V}_{\text{enc}} \cdot \hat{\mathbf{R}}_{\text{enc}})(-\mathbf{V}_{\text{enc}} \cdot \hat{\mathbf{R}}_{\text{enc}})$, where H is the Heaviside step function (Henon 1972).
2. We calculate the impact parameters which describe how close the perturber gets to the binary barycentre and either of the binary members ($i = 1, 2$), respectively, as

$$\mathbf{b} = \mathbf{R}_{\text{enc}} - \hat{\mathbf{V}}_{\text{enc}} \left(\mathbf{R}_{\text{enc}} \cdot \hat{\mathbf{R}}_{\text{enc}} \right), \quad (12)$$

$$\mathbf{b}_i = \mathbf{b} - \mathbf{R}_i - \hat{\mathbf{V}}_{\text{enc}} \left[(\mathbf{b} - \mathbf{R}_i) \cdot \hat{\mathbf{V}}_{\text{enc}} \right], \quad (13)$$

where \mathbf{R}_i are the positions of the binary members in the barycentre frame.

3. We add an instantaneous kick

$$\Delta v_i = \frac{2Gm_p}{V_{\text{enc}}} \frac{\hat{\mathbf{b}}_i}{b_i} \quad (14)$$

to the velocity of both binary members and update the barycentre velocity accordingly. In the impulsive approximation the instantaneous positions of the binary members and their barycentre remain unaffected.

We have modified **MSTAR** to include the kick prescription above. Typically, the integration step Δt of **MSTAR** is a small fraction of the orbital period of the binary and within this step it experiences $k \sim \mathcal{O}(1 - 1000)$ weak encounters.

2.4. Initial conditions

Using the integration scheme described above, we simulate the evolution of a population of 10^5 wide binaries whose initial parameters (denoted with subscript “0”) are as follows. The semi-major axes a_0 are drawn from a log-uniform distribution between 10^2 and 10^5 AU and the eccentricities from a thermal distribution $p(e_0) \propto e_0$

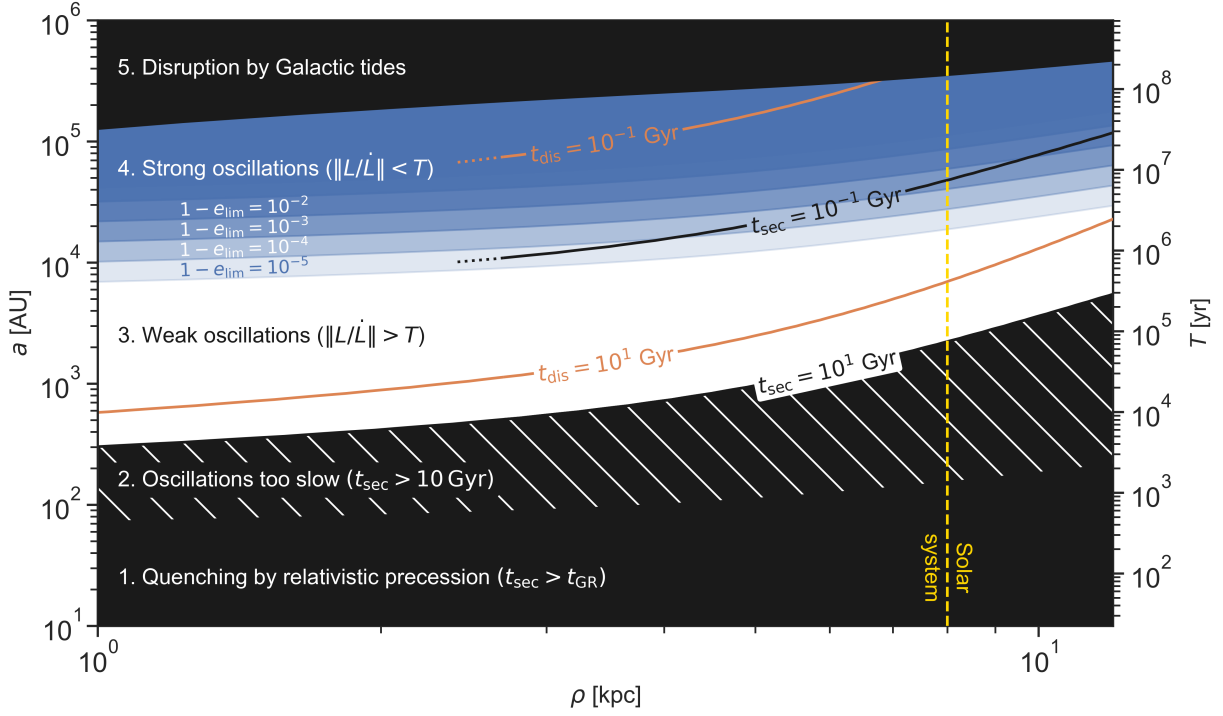


Figure 2. Five different dynamical regimes for wide binaries inside the Milky Way potential. We assume an example binary with semi-major axis a whose barycentre moves on a circular trajectory at a Galactocentric radius ρ on the Galactic plane. We set the binary masses to $m_1 = m_2 = 1 M_\odot$ but note that the displayed dynamical regimes are not particularly sensitive to this choice. The figure shows that our sampled range, $a = 10^2 - 10^5$ AU (see Sec. 2.4), fully covers the spectrum where the Galactic potential can influence wide binaries on a meaningful timescale. The details of the figure are fully explained in Sec. 3.

between 0 and 1. Our choice of the semi-major axis range roughly corresponds to the regime where secular changes of the binaries could be induced within a Hubble time, see Sec. 3 for details. While in reality the mass distributions of wide low-mass and high-mass stellar binaries and binaries of compact objects may significantly differ from each other (Moe & Di Stefano 2017; El-Badry 2024) we opt to choose a mass function which is as simple as possible in order to unbiasedly focus on its consequences for the dynamics. Thus, the component masses $m_{1,2}$ are independently sampled from a uniform distribution between 1 and $10 M_\odot$ which covers the typical masses of solar- to B-type stars and the peak of the mass distribution of binary black hole mergers inferred from gravitational-wave detections (Abbott et al. 2023). We discuss in Sec. 5 how plausible it is to form wide binary black holes from wide massive binary stars.

The orientation of the binary orbits with respect to the Galaxy are sampled isotropically, i.e., the initial argument of periastris ω_0 , longitude of the ascending node Ω_0 , cosine of the inclination $\cos i_0$, and orbital phase f_0 are sampled randomly and define the initial positions

and velocities of the binaries as (Merriitt 2013)

$$\mathbf{r}_0 = r_0 [\mathbf{u}_1 \cos(f_0 + \omega_0) + \mathbf{u}_2 \sin(f_0 + \omega_0)], \quad (15)$$

$$\dot{\mathbf{r}}_0 = \sqrt{\frac{Gm}{p_0}} \{ -\mathbf{u}_1 [e_0 \sin \omega_0 + \sin(f_0 + \omega_0)] + \mathbf{u}_2 [e_0 \cos \omega_0 + \cos(f_0 + \omega_0)] \}, \quad (16)$$

where $p_0 = a_0(1 - e_0^2)$ and $r_0 = p_0/(1 + e_0 \cos f_0)$ and

$$\mathbf{u}_1 = \begin{pmatrix} \cos \Omega_0 \\ \sin \Omega_0 \\ 0 \end{pmatrix}, \quad \mathbf{u}_2 = \begin{pmatrix} -\cos i_0 \sin \Omega_0 \\ \cos i_0 \cos \Omega_0 \\ \sin i_0 \end{pmatrix}. \quad (17)$$

The Galactocentric positions and velocities of the binary barycentres are initialised using `cogsworth`² (Wagg et al. in prep.) which is based on the Galaxy model of Wagg et al. (2022). This is an empirically informed model of the metallicity-dependent star formation history of the Milky Way in a low- α and high- α disc and bulge component (McMillan 2011; Bovy et al. 2016, 2019; Frankel et al. 2018). We initialise the trajectory of the binary barycentre within the Galaxy based on its

² <https://cogsworth.readthedocs.io/>

initial position, such that the initial velocity is equal to its circular velocity in the Milky Way potential with an additional isotropic 5 km s^{-1} dispersion (Price-Whelan 2017; Price-Whelan et al. 2024).

The evolution of the binaries which are initiated in this way is simulated twice. In one simulation we focus exclusively on the influence from Galactic tides (Sec. 2.2) and ignore the effect of stellar encounters (Sec. 2.3). In the other simulation we repeat the integration of each system but consider the combined effect of Galactic tides and stellar encounters. In either case, the binaries are evolved for a maximum integration time $t_{\text{max}} = 14 \text{ Gyr}$ unless they merge earlier due to the emission of gravitational waves or are disrupted in the sense that their semi-major axis becomes larger than the initial value by a factor of ten. Binaries that would undergo a collision or mass transfer if they were made of stars are identified by post processing the data as described below in Sec. 3.

3. RESULTS

A wide binary and its host galaxy can be viewed as an effective hierarchical triple in which the “inner” orbit of the binary members around each other and the much larger “outer” orbit of the binary barycentre in the Galaxy exchange orbital angular momentum (e.g., Naoz 2016). Similar to actual triples the tidal torque exerted along the “outer” orbit inside the Galactic potential can induce incremental changes of the binary angular momentum $L \propto \sqrt{1 - e^2}$ per “inner” orbital period. Over longer timescales these changes can accumulate and give rise to large-amplitude oscillations of the binary eccentricity e which determines how close and far the two binary members get at peri- and apoapsis $r = a(1 \mp e)$, respectively. This dynamical mechanism is studied in detail in the following subsections. In order to facilitate this investigation, we outline in Fig. 2 the most relevant dynamical regimes for wide binary evolution which are as follows:

1. *Quenching by relativistic precession:* In close binaries located in the lower black-shaded area ($a \lesssim \mathcal{O}(10^2) \text{ AU}$), the effect of the Galactic tides is suppressed by the “fast” relativistic precession of the binary orbit (Schwarzschild 1916). Formally, this is the case when the so-called secular timescale t_{sec} at which the Galaxy perturbs the binary (which we define in Sec. 3.1) exceeds the precession timescale $t_{\text{GR}} = a^{5/2} c^2 / 3G^{3/2} m^{3/2}$ (e.g., Liu et al. 2015).
2. *Oscillations too slow:* If the semi-major axis is a few 10^2 AU (hatched area), the Galaxy-induced eccentricity oscillations are no longer quenched by relativistic effects but occur on a long timescale

$t_{\text{sec}} > 10^1 \text{ Gyr}$ which renders them inefficient at perturbing the binary within a Hubble time.

3. *Weak oscillations:* In the white-shaded region, the torques do act on a timescale shorter than the Hubble time but it is much longer than the orbital period ($\|L/\dot{L}\| > T$). In this regime, they can incrementally perturb the binary orbit-by-orbit and slowly remove (or return) the binary orbital angular momentum (secular approximation). As a result, the Galactic torques give rise to regular long-term eccentricity oscillations whose amplitudes are relatively mild (typically $1 - e \gtrsim 10^{-4}$), unless the binary orbital plane is near-perpendicular to the Galactic plane in which case extreme eccentricities are possible.
4. *Strong oscillations:* In the blue-shaded regime, the torques act on a timescale shorter than the orbital period ($\|L/\dot{L}\| < T$). This corresponds to a “secular break-down” which renders the secular approximation formally inapplicable. As a result, we find that extreme eccentricity excitations are possible regardless of the binary inclination. The exact boundary of this regime depends on the current eccentricity of the binaries. Those which are already eccentric can be further driven towards extreme eccentricities more easily, which is indicated by the light-blue shading ($e = e_{\text{lim}}$).
5. *Disruption by Galactic tides:* Ultra-wide binaries located in the upper black-shaded region ($a \gtrsim \mathcal{O}(10^5) \text{ AU}$) tend to be ripped apart quickly by the Galactic tides (Hill instability) and are therefore short-lived (Jiang & Tremaine 2010).

In summary, the parameter space of interest where Galactic torques can induce significant eccentricity oscillations of binaries on a meaningful timescale is defined by the regimes 3 and 4 which are separately investigated in the following two subsections 3.1 and 3.2. In the entire parameter space the timescale t_{dis} (orange solid lines) for disruption due to the cumulative effect of encountering stars (Binney & Tremaine 2008) is longer than t_{sec} which indicates that Galactic tides have typically enough time to significantly perturb the binary orbit before a disruption due to stellar encounters could take place. We study the effect of the latter in the subsections 3.3 and 3.4.

3.1. Weak oscillations

Panel A of Fig. 3 shows an example of a wide binary whose binary separation oscillates between $r \approx 2 \times 10^4$ and 1 AU while its barycentre moves on a trajectory shown in panel B (edge-on) and panel C (face-on) at a

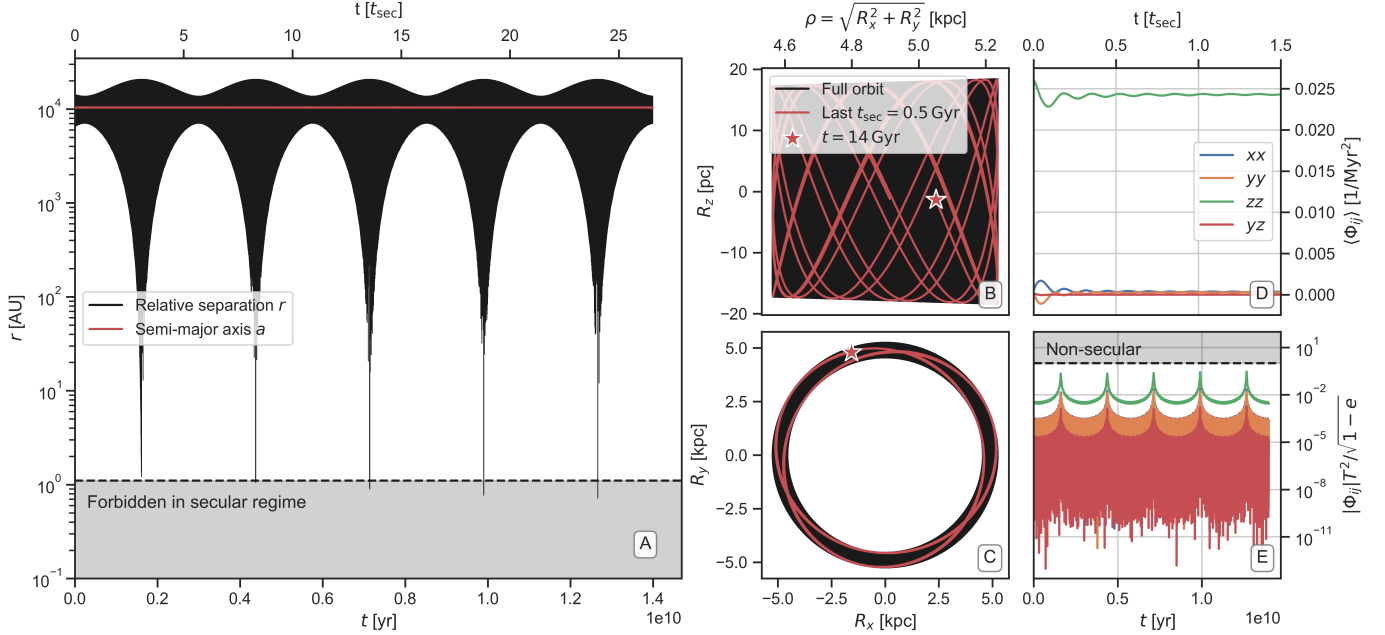


Figure 3. Example of a wide binary orbiting inside the Milky Way potential without stellar encounters. panel A: Relative separation r of the binary members and semi-major axis a as a function of time. The grey-shaded area is defined by $r < a(1 - e_{\text{max,sec}})$ where $e_{\text{max,sec}}$ is given by Eq. (19). For the secondary abscissa we calculate the secular timescale t_{sec} from Eq. (20). Panels B and C: The trajectory of the binary barycentre viewed edge-on and face-on, respectively. The black curve shows the entire trajectory over $t = 14$ Gyr, red highlights the last $t \in [14 \text{ Gyr} - t_{\text{sec}}, 14 \text{ Gyr}]$ of it, and the star symbol indicates the final ($t = 14 \text{ Gyr}$) position of the binary. panel D: The time-average $\langle \Phi_{ij} \rangle(t)$ of the tidal field components along the barycentre trajectory. Off-diagonal terms not shown here are zero or quickly decay to it. Panel E: The variations of the tidal field to check for the secular break-down condition in Eq. (28). The grey-shaded area defines the parameter space where the condition is satisfied and large non-secular eccentricities are possible.

Galactocentric radius of $\rho = \sqrt{R_x^2 + R_y^2} \approx 5 \text{ kpc}$ near the Galactic plane ($R_z \lesssim 20 \text{ pc}$). Additionally, panels D and E display information about the components of the tidal field $\Phi_{ij} = \partial^2 \Phi / \partial x_i \partial x_j$ (where $x_1 = x$, $x_2 = y$, and $x_3 = z$) along the barycentre trajectory which determine the leading-order contribution to the Galactic acceleration \mathbf{f}_i in Eq. (3). Panel D shows how the time-average

$$\langle \Phi_{ij} \rangle(t) = \frac{1}{t} \int_0^t \Phi_{ij}(\mathbf{R}(t')) dt' \quad (18)$$

evolves along the trajectory $\mathbf{R} = \mathbf{R}(t)$ for $t > 0$. In panel E we show the instantaneous components $\Phi_{ij}(t) = \Phi_{ij}(\mathbf{R}(t))$ (in units of $\sqrt{1-e}/T^2$) along the trajectory.

For this system, the angular frequencies $\dot{\Omega}_\rho$, $\dot{\Omega}_\phi$ and $\dot{\Omega}_z$ of the barycentre trajectory along the radial, azimuthal, and vertical direction, respectively, are much higher than the frequency $1/t_{\text{sec}}$ (defined below) of secular changes of the orbital elements and they are non-commensurable, i.e., the binary traces a non-repeating path through the Galaxy (Binney & Tremaine 2008). As a consequence, the trajectory of the binary barycentre densely fills an axisymmetric torus within a few t_{sec} and the leading-order perturbation of the binary can be approximately determined by the torus-average

of the tidal field $\langle \Phi_{ij} \rangle$ over many azimuthal periods. This situation was generally studied by Hamilton & Rafikov (2019a,b, 2021) who showed that the torus-averaged tidal field is diagonal ($\langle \Phi_{ij} \rangle = 0$ for $i \neq j$ and $\langle \Phi_{xx} \rangle = \langle \Phi_{yy} \rangle$; see panel D) and admits an integral of motion $\Theta = (1 - e^2) \cos^2 i$. Thus, the eccentricity and the binary orientation oscillate at the expense of each other, with the eccentricity reaching a maximum given by

$$1 - e_{\text{max,sec}}^2 = \frac{\Sigma + \sqrt{\Sigma^2 - 10\Gamma\Theta(1 + 5\Gamma)}}{1 + 5\Gamma}, \quad (19)$$

on a characteristic timescale

$$t_{\text{sec}} = \frac{4\pi}{3T\langle \Phi_{zz} + \Phi_{xx} \rangle}, \quad (20)$$

where

$$\Gamma = \frac{1}{3} \frac{\langle \Phi_{zz} \rangle + \langle \Phi_{xx} \rangle}{\langle \Phi_{zz} \rangle - \langle \Phi_{xx} \rangle}, \quad (21)$$

$$\Sigma = \frac{1 + 5\Gamma}{2} + 5\Gamma\Theta + \left(\frac{5\Gamma - 1}{2} \right) D, \quad (22)$$

$$D = e^2 \left(1 + \frac{10\Gamma}{1 - 5\Gamma} \sin^2 i \sin^2 \omega \right). \quad (23)$$

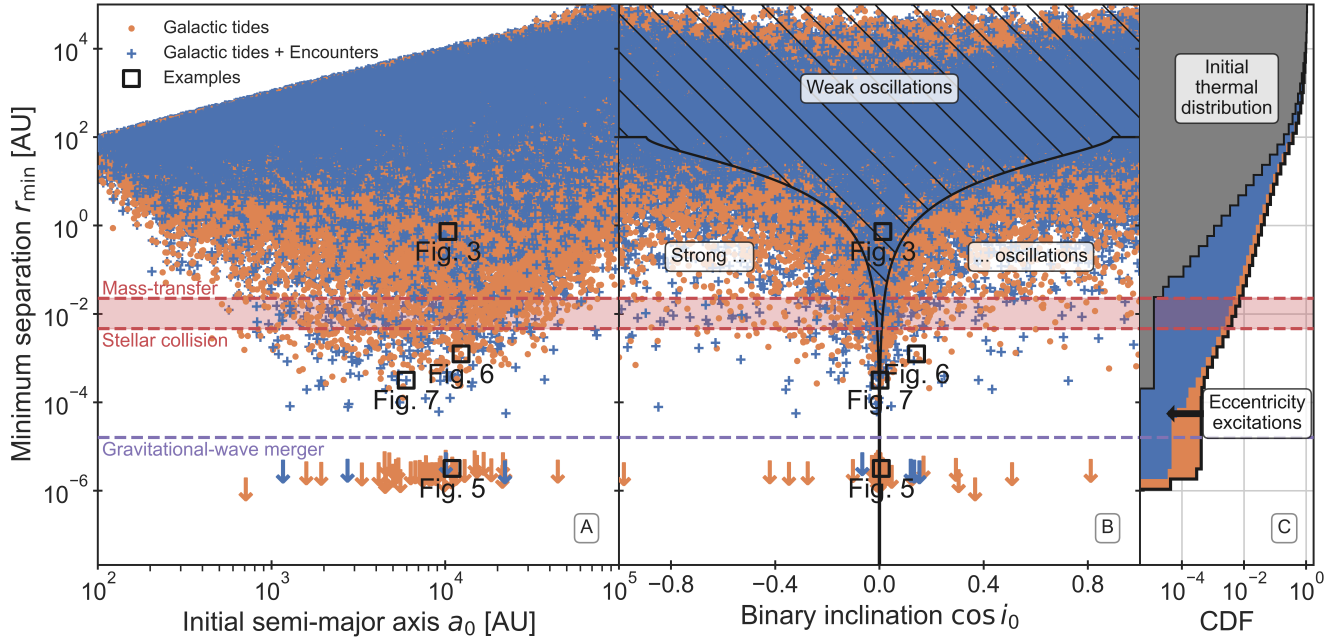


Figure 4. The effect of Galactic tides in driving wide binaries to close separations. Panels A and B show the minimum separation r_{\min} of the binaries in our population as a function of their initial semi-major axis a_0 and the initial inclination $\cos i_0$ between their orbital plane and the Galactic plane, respectively. The minimum separation r_{\min} is defined as the closest distance the binary members ever achieve due to Galactic tides over a maximum integration time of 14 Gyr, either when considering (orange dots) or when neglecting (blue crosses) encounters with passing stars. The purple dashed line separates compact object binaries that merge due to the emission of gravitational waves, where arrows indicate that the binaries are simulated until merging. The red-shaded area shows the regime in which stellar binaries fill their Roche-lobes at periastris (Eggleton 1983); below that area they potentially collide. The black line in panel B forms a narrow cone defining the smallest minimum separation allowed in the torus-averaged approximation (Eq. (19)) for a fiducial semi-major axis $a_0 = 10^2$ AU. Black squares indicate particular example systems shown in Figs. 3 and 5 – 7. Panel C shows the cumulative distribution functions (CDF) as well as the initial distribution of $r_{\min} = a_0(1 - e_0)$ following a thermal eccentricity distribution (see Sec. 2.4).

For our barycentre trajectories we typically find that $\Gamma \approx 1/3$ which agrees with the analytical result for epicyclic orbits in disk-like potentials (Hamilton & Rafikov 2019c). Thus, in the torus-filling approximation the maximum of the eccentricity and the timescale of oscillations can be calculated from the initial values of e, i , and ω and the average $\langle \Phi_{ii} \rangle$ along the barycentre trajectory. We numerically verify that the example system shown in Fig. 3 satisfies this approximation as the timescale for oscillations agrees with t_{sec} within a factor of order unity and the minimum separation is limited by $r \gtrsim a(1 - e_{\text{max,sec}})$ (indicated by the grey-shaded area in panel A).

In general, reaching extreme eccentricities in the torus-filling approximation is confined to a narrow window around $\cos^2 i_0 \approx 0$, i.e., binaries whose orbital plane is near-perpendicular to the Galactic plane. Indeed, considering initially circular binaries ($e_0 = 0$) Eq. (19) simplifies to

$$e_{\text{max,sec}} = \sqrt{1 - \frac{10\Gamma}{1 + 5\Gamma} \cos^2 i_0}, \quad (24)$$

which, e.g., for a typical value of $\Gamma \approx 1/3$ requires $|\cos i_0| \lesssim 1.6 \times 10^{-4}$ to reach an eccentricity as large as $e_{\text{max,sec}} \gtrsim 1 - 10^{-4}$ like the one presented in Fig. 3.

In Fig. 4, we show the minimum separations of our entire binary population, as a function of their initial semi-major axis and the initial mutual inclination with respect to the Galaxy. Here, we focus on the model where we include only the effect of Galactic tides (blue) and investigate the additional effect of stellar encounters (orange) in Sec. 3.3. Considering the dependence of the minimum separation on the initial relative inclination (panel B), we see that the majority of systems are roughly consistent with the maximum eccentricity predicted by the torus-averaged approximation (cf. Eqs. (19)). They show a characteristic concentration of large eccentricities around initial inclinations $\cos i_0 \approx 0$, defining a narrow cone of inclinations within which large eccentricity excitations are possible in the torus-averaged approximation. As a reference, the minimum separation in the torus-averaged approximation is

shown for initially circular binaries ($e_0 = 0$) at our smallest initial semi-major axis $a_0 = 10^2$ AU (black line).

3.2. Strong oscillations

The torus-filling approximation described in the previous subsection fails to characterise the systems which undergo the strongest eccentricity oscillations and attain the smallest separations in our population. Instead, Fig. 4 shows that high eccentricities are achieved well beyond the narrow cone of initial inclinations predicted by the torus-filling approximation. Depending on the type of wide binary these high-eccentricity excitations can have important evolutionary implications. A few 0.1 % of the binaries in our population are driven to $r_{\min} < R_\odot$ (red dashed line) where we would expect a stellar collision if the wide binary was composed of two solar-type main-sequence stars (cf., Kaib & Raymond 2014). In stellar binaries reaching $r_{\min} \gtrsim R_\odot$ (red-shaded area) one or both members will fill their Roche-lobe at periastris (Eggleton 1983) and transfer mass to their companion which may give rise to electromagnetic signals. About a few 0.01 % of the binaries are driven to separations which inevitably lead to a subsequent inspiral due to gravitational-wave emission (purple dashed line). If these binaries are composed of black holes or neutron stars their inspiral will lead to a merger that could result in a multi-band gravitational-wave detection (see below). Towards $a_0 \sim 10^5$ AU we observe a depletion of large eccentricities because these loosely bound systems tend to be quickly disrupted by the pull of the Galactic tides (see Sec. 3.4).

Panel C of Fig. 4 shows that the resulting fraction of extremely eccentric binaries leading to the aforementioned evolutionary outcomes are neither expected from the initial thermal distribution nor in the torus-filling approximation. Instead, we identify two reasons leading to a break-down of the latter and to extreme eccentricity excitations which are as follows.

Firstly, the maximum eccentricity in the torus-filling approximation is derived from a torus-averaged potential in which any short-term variation of Φ_{ij} is washed out. In reality, there are small but non-zero residuals $\delta\Phi_{ij} = \Phi_{ij} - \langle\Phi_{ij}\rangle$ along the trajectory of the binary barycentre which are neglected in the torus-averaged approximation. These residuals are peculiar near a high-eccentricity peak where the binaries only carry a tiny orbital angular momentum $L \propto \sqrt{1-e^2}$. Thus, even a small $\delta\Phi_{ij}$ could give rise to a torque which changes L by the order of itself. For hierarchical triples in which the binary is perturbed by the tidal field of a distant tertiary companion it is well-known that these residuals can result in a different maximum eccentricity than predicted

from an orbit-averaged potential (Antonini et al. 2014; Luo et al. 2016; Antonini et al. 2017; Grishin et al. 2018; Hamilton & Rafikov 2024). For binaries moving in some arbitrary potential, we generalise previous findings and estimate the importance of this effect by considering the instantaneous torque exerted by the Galactic potential

$$\frac{d\mathbf{L}}{dt} = -\mu\mathbf{r} \times \nabla\Phi|_{\mathbf{R}+\mathbf{r}}. \quad (25)$$

Introducing a set of orthonormal basis vectors $\hat{\mathbf{e}}_r$, $\hat{\mathbf{e}}_L$, and $\hat{\mathbf{e}}_p$ that point along the relative separation of the binary, its orbital angular momentum, and a vector which is orthogonal to the latter two, respectively, the leading-order (quadrupole) contribution to the torque can be written as

$$\frac{d\mathbf{L}}{dt} = \mu r^2 (\Phi_{rp}\hat{\mathbf{e}}_L - \Phi_{rj}\hat{\mathbf{e}}_p), \quad (26)$$

where the potential derivatives Φ_{rp} and Φ_{rj} are evaluated at \mathbf{R} . The torque is maximised at apoapsis $r = a(1+e)$ where in the limit $e \rightarrow 1$ the timescale for changes in $L = \|\mathbf{L}\|$ evaluates to

$$\left\| \frac{1}{L} \frac{dL}{dt} \right\|^{-1} = \frac{\pi}{\sqrt{2}} \frac{\sqrt{1-e}}{T\|\Phi_{rp}\|}. \quad (27)$$

If this timescale is shorter than the orbital period T any secular treatment in which the potential is averaged over the orbital period or the “outer” period inside the Galaxy ($1/\dot{\Omega}_\rho$, $1/\dot{\Omega}_\phi$, or $1/\dot{\Omega}_z$) formally breaks down (c.f., Hamilton & Rafikov 2019a,b; Bub & Petrovich 2020; Hamilton & Rafikov 2021; Rasskazov & Rafikov 2023) and must be replaced by a direct N -body integration like the one presented in this study. The condition for secular break-down can be rewritten in compact form as

$$\sqrt{1-e} \lesssim T^2 \|\Phi_{rp}\|, \quad (28)$$

where for some arbitrary orientation of the orbital frame $(\hat{\mathbf{e}}_r, \hat{\mathbf{e}}_p, \hat{\mathbf{e}}_L)$, $\|\Phi_{rp}\|$ can be as large as $\sim \max_{i,j=x,y,z}(\|\Phi_{ij}\|)$. Eq. (28) generalises the condition found by Antonini et al. (2014) for hierarchical triples to arbitrary perturbing potentials. One recovers the former by explicitly using $\Phi = -Gm_3/a_{\text{out}}(1-e_{\text{out}})$ where m_3 is the mass of the tertiary companion and $a_{\text{out}}(1-e_{\text{out}})$ is the periastris of its orbit around the inner binary barycentre.

In panel E of Fig. 3 we can see that the previous example binary remains in the secular torus-filling regime as condition (28) remains unfulfilled and Eq. (19) accurately describes the maximum eccentricity. In contrast, we show in Fig. 5 a binary which is torus-filling in the sense of Sec. 3.1 but whose evolution satisfies Eq. (28) and becomes non-secular near the high-eccentricity peak

at $t \approx 2.3$ Gyr. As a consequence, the tidal field torques the binary to an extreme eccentricity $1 - e_{\max} \approx 10^{-8}$ where at periastris gravitational wave radiation decouples the binary from the Galactic perturbation and causes an orbital decay and circularisation through the bandwidths of LISA and LIGO/Virgo/Kagra towards a merger (inset to panel A).

We stress that substituting $\|\Phi_{rp}\| \rightarrow \max_{i,j=x,y,z}(\|\Phi_{ij}\|)$ in Eq. (28) must be seen as an order-of-magnitude calculation for the occurrence of high eccentricities due to secular break-down. In practice, the accuracy of the substitution for individual systems could be limited due to the facts that (i) the sign of Φ_{rp} may actually cause a torque to lower eccentricities, (ii) writing Φ_{rp} in terms of $\Phi_{i,j=x,y,z}$ with respect to the coordinates depends on the actual orientation of the binary, and (iii) Eq. (28) was derived from the instantaneous torque at apoapsis and does not guarantee that the binary maintains its (high) eccentricity value until the subsequent pericentre passage, but also (iv) the torus-filling approximation already fails if the timescale (27) is less than the “outer” period $\sim 1/\dot{\Omega}_\phi$ inside the Galaxy (which is generally much longer than the binary period T). Nevertheless, we find that satisfying Eq. (28) to undergo secular break-down correlates well with the systems which experience extreme eccentricities that can no longer be described by the torus-filling approximation.

The second reason for which the torus-filling approximation can break down is the emergence of chaos. The previous examples are characterised by $\dot{\Omega}_\phi t_{\text{sec}} \gg 1$ in which case within a secular timescale the tidal tensor components Φ_{ij} quickly converge to their torus-average, $\langle \Phi_{xx} \rangle = \langle \Phi_{yy} \rangle$, and $\langle \Phi_{ij} \rangle = 0$ for $i \neq j$ (panel D of Fig. 3 and 5). As shown by Hamilton & Rafikov (2019a,b, 2021) this results in regular cycles of secular changes on a timescale $\mathcal{O}(t_{\text{sec}})$. In contrast, the evolution can become chaotic if the azimuthal period of the barycentre becomes comparable to the secular timescale ($\dot{\Omega}_\phi t_{\text{sec}} \approx 1$) an example of which is shown in Fig. 6. In that case, the averaged tidal tensor components fail to converge even on many secular timescales t_{sec} (panel D) and the binary undergoes a random walk through phase space which eventually leads to extreme eccentricities. Equivalent findings were made for hierarchical triples and quadruples and binaries orbiting inside a cluster potential (Petrovich & Antonini 2017; Hamers & Lai 2017; Liu & Lai 2019; Bub & Petrovich 2020).

3.3. Effect of stellar encounters

Considering the effect of stellar encounters, panel C of Fig. 4 shows that their inclusion marginally reduces

the number of high-eccentricity excursions in our population. Comparing the simulations with and without stellar encounters, we find the numbers of stellar collisions ($r_{\min} < R_\odot$) and gravitational-wave mergers get reduced by factors of ~ 2 and 5, respectively. It is noteworthy that we find almost no system which undergoes a stellar collision or gravitational-wave merger in both models. Instead, the actual evolutionary outcome is randomised. This is due to the fact that stellar encounters at each timestep add a small random perturbation to the relative velocity of the binary (see Sec. 2.3) which may either break a resonance that would have led to a high eccentricity due to Galactic tides alone or may actually be the cause that placed it on a resonant orbit. An example is shown in Fig. 7 where the binary undergoes large-eccentricity excitation on a resonant highly inclined trajectory ($\cos i_0 \approx 0$, see panel B of Fig. 4) until a stellar encounter at $t \approx 1.5$ Gyr breaks the resonance and quenches further perturbation. Finally, another encounter at $t = 9.0$ Gyr disrupts the binary. Disrupting binaries are studied in the following Sec. 3.4.

3.4. Disruptions

Owing to their low binding energy, wide binaries are susceptible to disruptions by Galactic tides and the (cumulative) effect of stellar encounters, which we find is the case for around 10% of the binary population in either simulation. A useful quantity to understand whether a binary can get disrupted by the Galactic tides is set by the Jacobi radius r_J given by (Binney & Tremaine 2008; Jiang & Tremaine 2010)

$$r_J(\rho) = f(\rho) \left[\frac{m}{3M(\rho)} \right]^{1/3} \rho, \quad (29)$$

where

$$f(\rho) = \left[1 - \frac{1}{3} \frac{d \ln M(\rho)}{d \ln \rho} \right]^{1/3}, \quad (30)$$

and $M(\rho)$ is the mass of the Galaxy interior to ρ . The Jacobi radius given by Eqs. (29) and (30) defines the maximum extent of a satellite body orbiting on a circular trajectory inside a spherically symmetric host (Binney & Tremaine 2008). Our host Galaxy is neither spherically symmetric nor do we restrict our binary barycentres to circular trajectories. Nevertheless, we find that r_J evaluated at the minimum Galactocentric radius $\rho_{\min} = \min(\rho(t))$ along the barycentre trajectory demarcates well the region of stability of our simulated binaries. This is shown in Fig. 8 where the apoapsis of most disrupted binaries exceeds the Jacobi radius at their minimum Galactocentric radius ($r \approx 2a_0 > r_J$; solid/dashed lines). This result confirms previous findings of Jiang & Tremaine (2010) who found that $r \sim$

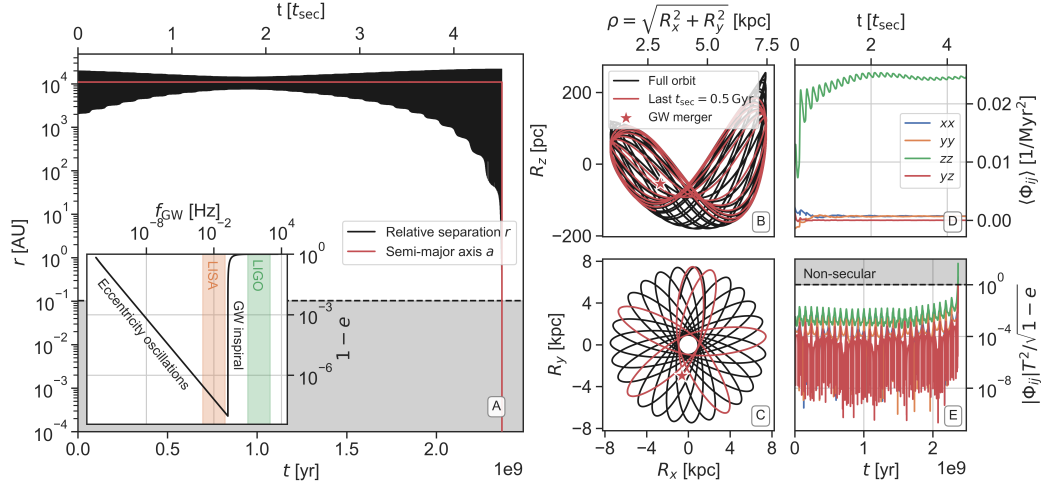


Figure 5. Same as Fig. 3 for a binary undergoing a non-secular high-eccentricity excitation after $t \approx 2.3$ Gyr followed by a gravitational-wave merger. The inset to panel A displays the evolution of the binary eccentricity e and the dominant harmonic of the gravitational-wave frequency f_{GW} (Wen 2003) through the bandwidths of LISA and LIGO/Virgo/Kagra.

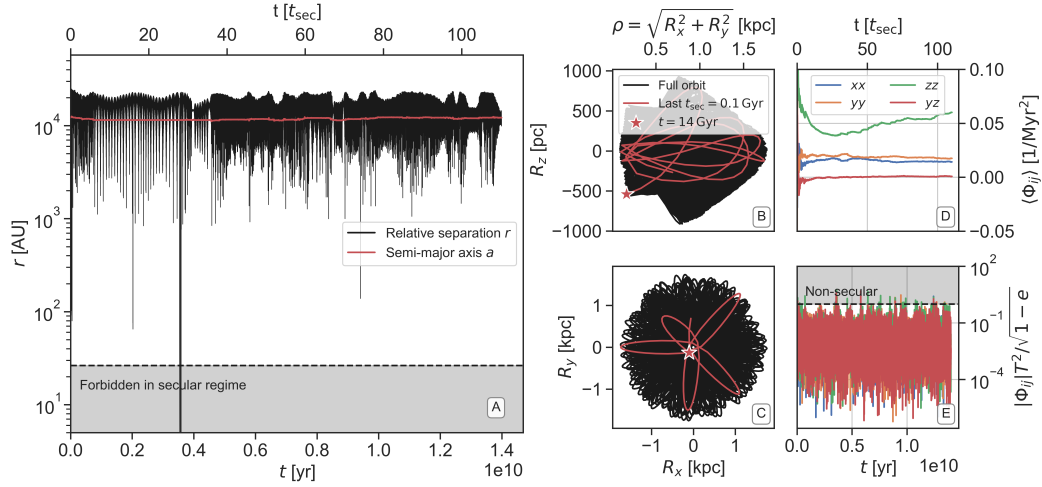


Figure 6. Same as Fig. 3 for a binary undergoing chaotic evolution.

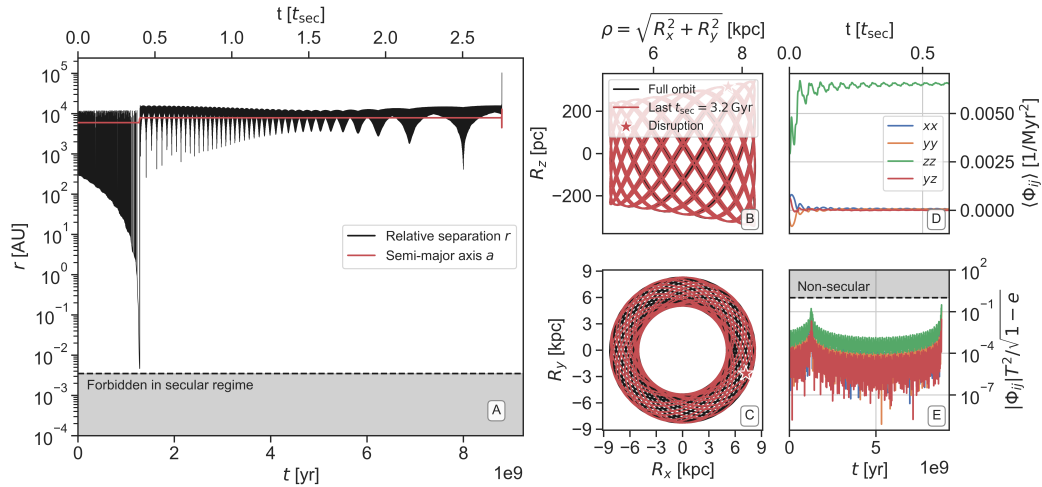


Figure 7. Same as Fig. 3 for a binary that is perturbed by stellar encounters and which gets disrupted after $t \approx 9$ Gyr.

$\mathcal{O}(r_J)$ sets a natural limit to the stability of wide binaries in the solar neighborhood.

Fig. 8 shows that exceptions to this stability criterion only occur if stellar encounters are taken into account. In that case, the velocity kicks imparted to the binary members can occasionally unbind them even if they are much closer to each other than the stability limit defined by the Jacobi radius.

4. RATE CALCULATIONS

Here, we estimate the galaxy-driven volumetric event rate of binary black hole (BBH) mergers, collisions of stars on the main-sequence (MSMS), and of binary white dwarfs (BWDs) in the local Universe. For this purpose, we adopt a simplistic formalism and do an order-of-magnitude estimate of the rate in the flavour of a Drake equation, which for BBH mergers reads

$$\begin{aligned} \mathcal{R}_{\text{BBH}} = & \underbrace{\rho_{\text{MW}}}_{\text{Number density MW-like galaxies}} \times \underbrace{N_{\text{MW}}}_{\text{Number of stars in MW}} \\ & \times \underbrace{A}_{\text{Massive primary fraction}} \times \underbrace{B}_{\text{Companion fraction}} \\ & \times \underbrace{C}_{\text{Massive companion fraction}} \times \underbrace{D}_{\text{Wide BBH formation fraction}} \\ & \times \underbrace{E}_{\text{Galaxy-driven merger fraction}} \times \underbrace{\frac{1}{14 \text{ Gyr}}}_{\text{per max. integration time}}. \end{aligned} \quad (31)$$

We assume that the number density of Milky Way-like galaxies is $\rho_{\text{MW}} = 0.0116 \text{ Mpc}^{-3}$ and that they host a total number of $N_{\text{MW}} = 1 - 4 \times 10^{11}$ stars (Kopparapu et al. 2008). Only a fraction A of all stars is massive enough to form a black hole. Adopting a lower limit of $20 M_{\odot}$ and a Kroupa (2001) initial mass function between 0.08 and $150 M_{\odot}$ this fraction evaluates to $A = 1.3 \times 10^{-3}$. The large majority $B = 0.94$ of massive stars is accompanied by another star (Moe & Di Stefano 2017). In this calculation, we do not distinguish between companions that form an isolated binary, triple, or higher-order configuration and discuss this approximation in Sec. 5. Again, only a fraction C of the companions is massive enough to form a black hole too. Because we are interested in the formation of wide BBHs, we can draw the mass ratio $q = m_2/m_1$ from the observed distribution $p(q) \propto q^{-2}$ between 0.1 and 1.0 for long-period binaries, which is nearly consistent with an independent sampling of the companion mass from the initial mass function (Moe & Di Stefano 2017). Thus, we find for the fraction in which both stars are massive ($m_{1,2} > 20 M_{\odot}$) $A \times C = 1.3 \times 10^{-4}$.

To estimate the fraction D of massive stellar binaries which successfully form wide BBHs in the simulated semi-major axis range $10^2 - 10^5 \text{ AU}$, we run a population of massive binaries ($m_{1,2} > 20 M_{\odot}$) from the zero-age-main-sequence with the rapid binary population synthesis code COMPAS (Riley et al. 2022). Since wide BBHs originate from non-interacting stars their fraction is fully determined by the stellar wind model and the natal kick prescription. Here, we follow Vink et al. (2001) for the winds and the “delayed” fallback supernova engine model of Fryer et al. (2012). Assuming a log-uniform semi-major axis distribution between 10^{-1} and 10^5 AU (Offner et al. 2023), a thermal eccentricity distribution between 0 and 1 (Moe & Di Stefano 2017), a Kroupa (2001) mass function for the primary star, and $p(q) \propto q^{-2}$ between 0.1 and 1.0 for the secondary, we find $D = 0.41$ and 0.37 at low ($Z = 2 \times 10^{-4}$) and high metallicity ($Z = 2 \times 10^{-2}$), respectively. Our simulations show that a fraction $E \approx 5 \times 10^{-5}$ of these are driven to a gravitational-wave merger by the Galactic perturbation (see panel C of Fig. 4). These assumptions result in a BBH merger rate $\mathcal{R}_{\text{BBH}} \approx 0.2 - 0.8 \text{ Gpc}^{-3} \text{ yr}^{-1}$ which amounts to a fraction $0.4 - 5 \%$ of the observed rate $17.9 - 44 \text{ Gpc}^{-3} \text{ yr}^{-1}$ (90 % C.L.) inferred from LIGO/Virgo/Kagra gravitational-wave detections (Abbott et al. 2023).

To estimate the rate of collisions $\mathcal{R}_{\text{MSMS}}$ of main-sequence stars we note that the wide binary fraction ($a \gtrsim 10^2 \text{ AU}$) of low-mass stars ($m_1 = 0.3 - 5 M_{\odot}$) has been observed to be around 10 to 46% which we can use to replace $B \times C \times D$ in Eq. (31) (Offner et al. 2023). For a (Kroupa 2001) mass function, the fraction of primaries in the range $m_1 = 0.3 - 5 M_{\odot}$ evaluates to $A = 0.38$, and our simulation shows that a fraction $E \approx 2 \times 10^{-3}$ of binaries fall below $r_{\text{min}} < 1 R_{\odot}$. Thus, we infer a total rate $\mathcal{R}_{\text{MSMS}} \approx 0.6 - 11.6 \times 10^{-5} \text{ Mpc}^{-3} \text{ yr}^{-1}$ which is consistent with recent measurements of the rate $7.8^{+6.5}_{-3.7} \times 10^{-5} \text{ Mpc}^{-3} \text{ yr}^{-1}$ of Luminous Red novae (Karambelkar et al. 2023) and agrees with previous estimates from Kaib & Raymond (2014).

Lastly, for the rate of binary white dwarf collisions we simply reduce the previous rate estimate for MS collisions using $E \approx 5 \times 10^{-5}$ to account for the lower probability to get $r_{\text{min}} < 10^{-2} R_{\odot}$. In order to make a meaningful comparison to observations we additionally impose a minimum mass of the primary of $0.8 M_{\odot}$ for the collision to produce enough radioactive nickel to be visible as a type Ia SN, as also assumed by Ruiter et al. (2011). For the Kroupa (2001) mass function this introduces another reduction by a factor of 50 , so that \mathcal{R}_{BWD} amounts to a fraction $0.01 - 0.1 \%$ of the measured rate $4.1 \times 10^{-5} \text{ Mpc}^{-3} \text{ yr}^{-1}$ of Type Ia SNe (Toy et al. 2023).

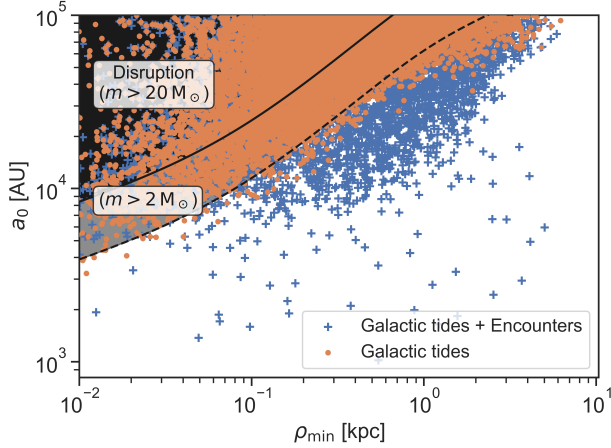


Figure 8. Initial semi-major axis a_0 and minimum Galactocentric radius ρ_{\min} of wide binaries which get disrupted. Disruptions are defined when the binary separation at any time in the simulation exceeds $r = 10a_0$ (see Sec. 2.1). The minimum Galactocentric radius ρ_{\min} is defined as the minimum of ρ of the barycentre trajectory inside the Galaxy. Grey- and black-shaded regions correspond to Hill instability evaluated at that distance for binary masses $m > 2 M_\odot$ and $m > 20 M_\odot$, respectively. These limits correspond to the minimum and maximum mass in our population (see Sec. 2.4).

We stress that Eq. (31) leads to an order-of-magnitude rate estimate that takes into account neither how different other potentials than the Milky Way contribute (see Sec. 5), nor how the merger fraction depends on the mass of the binary members. Furthermore, it does not properly convolve the star-formation rate as a function of time with the delay time distribution for a particular event. A more accurate rate estimate, which specifically depends on the type of event, is beyond the scope of this paper and should be addressed in the future. However, we have checked that the merger fraction is nearly independent of the input masses of the binaries and that the typical delay time of the events, which is a few Gyr, coincides with the lookback time of the peak in star formation (Madau & Dickinson 2014).

5. CONCLUSIONS

In this study, we have shown that the torque exerted by the gravitational potential of the Milky Way can induce eccentricity oscillations of wide binaries orbiting inside the Galactic field. Largely relying on one or more of the assumptions 1 – 3 in Sec. 1, this has been known for decades (e.g., Heisler & Tremaine 1986) but we find that the maximum possible eccentricity excitation has been severely underestimated. By employing a direct N -body integrator which relies on none of the previous assumptions we have shown that near-unity eccentricities

($1 - e \lesssim 10^{-8}$) are possible in two different dynamical regimes. In the weak regime (Sec. 3.1) assumptions 1 – 2 are well-satisfied and large eccentricities are only possible within a narrow cone $\cos i_0 \approx 0$ of initial inclinations between the binary plane and Galactic plane (Fig. 4), similar to the von Zeipel-Kozai-Lidov effect in hierarchical triples (Naoz 2016) and binaries inside stellar clusters (Hamilton & Rafikov 2019a,b; Bub & Petrovich 2020; Hamilton & Rafikov 2021). This weak regime breaks down if the Galactic torque acts on a timescale less than the orbital period (Eq. (28)) or if chaos emerges when the binary orbits inside the Galaxy on a timescale similar to the secular timescale (Sec. 3.2). In either case, extreme eccentricities can be achieved beyond the cone of inclinations derived from the secular approximation. Depending on the type of wide binary, this dynamics may have important implications for the occurrence of stellar collisions, of white dwarf collisions, and binary black hole mergers and may contribute significantly to the observed rate of these events (Sec. 4).

We conclude this study by highlighting several aspects that need to be addressed in future work.

1. We have focused our investigation on binaries orbiting inside a Milky Way potential which was approximated as being axisymmetric and stationary (Sec. 2.1). It is not obvious whether including the non-axisymmetric and time-dependent density field of the Milky Way (including its bar and spiral structure) will change our findings. As with stellar encounters, it could either tend to break the resonance or introduce additional perturbations $\delta\Phi_{ij}$ of the tidal field (see Sec. 3.2) which may actually drive the binaries into the non-secular regime. Regarding other galactic potentials we do not have any reason to expect that the dynamical evolution would be qualitatively different. However, the potential of, e.g., elliptical, irregular, and dwarf galaxies, may significantly alter the fraction of each events quantitatively due to potentially different initial binary populations, the strength of Galactic torques, and the abundance of chaotic orbits. In addition, the time-evolution of such potentials could affect our results in a non-trivial way. In our analysis we find a relatively large span of delay times between the start of the simulation and the occurrence of a particular event. For instance, the gravitational-wave mergers cover a total range of delays between ~ 0.1 and 14.1 Gyr. The bulk of systems merge after a few Gyr, with a median value (75% – quantile) of 5.1 Gyr (10.5 Gyr), which, if contributing to the present-day local merger rate, would correspond to

- a birth redshift of $z \approx 0.5$ (2.0). Thus, a complete Galactic model would need to take into account the evolution over at least $0 \lesssim z \lesssim 2$.
2. When low-mass stars approach each other closely at periaapsis by the mechanism explored in this study, they interact with each other through stellar tides (e.g., Zahn 1975; Hut 1981). As shown by Kaib & Raymond (2014) the dissipated energy by tides can convert a wide binary at small periaapsis to a close or contact binary which is shielded against further perturbation from the Galaxy. Exploring a set of various tidal models for the (uncertain) amount of dissipated energy, Kaib & Raymond (2014) found that the formation of close binaries reduces the number of Galactically-driven stellar collisions by a factor of order unity, compared to no-tide evolution, for their fiducial dissipation models of polytropic stars (Lee & Ostriker 1986; Press & Teukolsky 1977) and a factor of around ten for some artificially extreme models. Thus, for any plausible tidal model, they find enough stellar mergers in their simulations to explain the observed rate of stellar collisions in the Milky Way. For the purpose of focusing on the point mass dynamics we have ignored the effect of tides in our work. Yet, applying the reduction factors found by Kaib & Raymond (2014) our rate of stellar collisions (Sec. 4) is lowered by a factor of a few at most.
 3. Unlike low-mass stars, their massive counterparts ($m_{1,2} \gtrsim 8 M_\odot$) evolve within a few Myr to neutron stars or black holes which is much shorter than the secular timescale t_{sec} at which the Galaxy could drive the binaries to a close periaapsis. Therefore, it is justified to neglect the effect of stellar tides for wide massive binaries. However, wide orbits of massive stars are found most often to be the outer orbit of a hierarchical triple or higher-order configuration (Moe & Di Stefano 2017), i.e., one or both wide binary members exhibit additional sub-companions. In addition, compact objects may experience a significant natal kick when they form from massive stars (Tauris & van den Heuvel 2023) which risks disrupting the loosely bound wide orbit. The effects of massive star multiplicity and natal kicks introduce uncertainties to our rate estimates of binary black hole mergers (Sec. 4). In general, natal kicks are caused by asymmetric mass ejection and neutrino emission during the core-collapse supernova explosions. It is thought that black holes tend to accrete all

the stellar material so that their kicks are mainly determined by the asymmetric neutrino emission leading to typical kicks of several km s^{-1} at most (Janka & Kresse 2024; Burrows et al. 2024), which is supported by recent observations of orbits hosting a black hole (Shenar et al. 2022; Vigna-Gómez et al. 2023; Burdge et al. 2024). Despite the kick uncertainties due to the exact explosion mechanisms and the amount of matter accreted onto the black hole (Mandel 2016), it is hence reasonable to assume that for many black holes the kick velocity is smaller than the typical orbital velocity of wide binaries (Eq. (11)) so that a significant number of wide massive binary stars successfully form wide binary black holes (Olejak et al. 2020). To estimate the impact of natal kicks on the formation of wide BBHs, we initiate a population of $N_0 = 10^5$ massive binary stars ($m_1 = m_2 = 10 M_\odot$) with a log-uniform semi-major axis distribution between 10^{-1} and 10^5 AU, a thermal eccentricity distribution, and isotropic orbital angles. We consecutively apply isotropic natal kicks at random orbital phases to each of the stars and update the orbital elements accordingly. The magnitude of the natal kicks is drawn from a Maxwellian velocity distribution with dispersion $\sigma_{\text{kick}} = 0.1, 0.5, 1.0, 5.0$, and 10.0 km s^{-1} , respectively. Figure 9 shows the final semi-major axis distribution of surviving BBHs indicating that for $\sigma_{\text{kick}} \lesssim \mathcal{O}(1) \text{ km s}^{-1}$ a significant fraction can be expected throughout the wide binary range explored in this work. Conversely, three-dimensional supernova simulations consistently predict large natal kicks for neutron stars (typically a few hundred km s^{-1}) which are mainly driven by the asymmetric mass ejection (Janka & Kresse 2024) and substantiated by the observation of high pulsar velocities (e.g., Hobbs et al. 2005). This is much larger than the typical orbital velocity of wide binaries which makes the successful formation of bound wide binary neutron stars or black hole-neutron star binaries extremely unlikely. Additionally, wide compact object binaries might form from initially unbound pairs of single objects due to chance encounters during the dissolution phase of young star clusters (Kouwenhoven et al. 2010).

4. Regarding multiplicity, while it is plausible that about 20 % of massive stellar triples and higher-order configurations could become wide binary black holes after the sub-companions are lost because of mergers during stellar evolution (Sana et al. 2012; Stegmann et al. 2022a), a non-

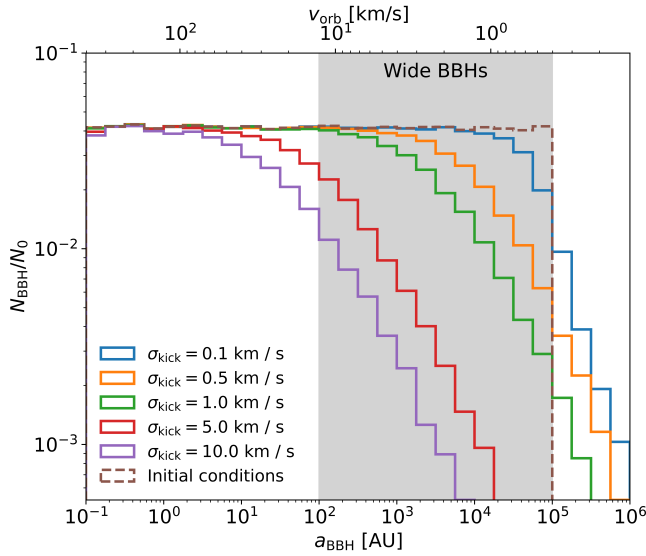


Figure 9. The effect of natal kicks on the formation of wide BBHs. The dashed line shows that the initial distribution of $N_0 = 10^5$ wide massive binaries ($m_1 = m_2 = 10 M_\odot$) which consecutively receive two natal kicks at BH formation whose magnitudes are drawn from a Maxwellian velocity distribution with dispersion σ_{kick} . Solid lines show the semi-major axis distribution of all surviving BBHs and the grey-shaded area highlights the range of values simulated in this work. As a reference, we also show the orbital velocity of the BBHs (Eq. (11)).

negligible number of wide binary black holes may form while retaining their sub-companions. Grishin & Perets (2022) have shown that a wide tertiary companion which is gently driven towards the inner binary through Galactic tides can trigger von Zeipel-Kozai-Lidov oscillations of the latter. For wide tertiary companions which are driven to a near-radial orbit through the mechanism studied in our work, we may additionally expect systems that undergo chaotic evolution at close periapsis passage similar to binary-single star scattering experiments (e.g., Samsing et al. 2014) which likely lead to the ejection of one of the components or the merger of two. Thus, we anticipate that the inclusion of additional tertiary or higher-order companions introduces further complexity to the problem, potentially enlarging the parameter space for mergers.

We emphasise that the proposed channel to form compact object mergers from wide binaries (or higher-order configurations with a wide outer orbit) is appealing from a theoretical point of view. Since the wide binary stars evolve far apart from each other, they are not subject to the systematic uncertainties associated with the stellar evo-

lution of interacting short-period massive binary stars that have been proposed to be the origin of compact object mergers; either through common-envelope evolution (Postnov & Yungelson 2014; Belczynski et al. 2016; Eldridge & Maund 2016; Lipunov et al. 2017), a stable mass transfer episode (van den Heuvel et al. 2017; Inayoshi et al. 2017; Neijssel et al. 2019; Bavera et al. 2021; Marchant et al. 2021; Gallegos-Garcia et al. 2021; Olejak et al. 2021; van Son et al. 2022), or chemically homogeneous evolution (de Mink & Mandel 2016; Mandel & de Mink 2016; Marchant et al. 2016; du Buisson et al. 2020; Riley et al. 2021). Instead, the uncertainty reduces to the initial properties and the formation of wide binaries (El-Badry 2024), the orbital widening due to mass-loss by stellar winds if the stars are metal-rich (Vink et al. 2001; Björklund et al. 2021), and to the remnant mass function and natal kick prescription of (effectively single) massive stars (Heger et al. 2003).

- Finally, we point out that it would be worthwhile to use our integrator to investigate the evolution of the eccentricity distribution of wide binaries in the solar neighbourhood. Tokovinin (2020) and Hwang et al. (2022) found that the wide binaries astrometrically identified in the *Gaia* DR2 sample show evidence for a super-thermal distribution, i.e., $p(e) \propto e^\alpha$ where $\alpha > 1$. Working with the secular approximation, Modak & Hamilton (2023) and Hamilton & Modak (2023) have shown that neither Galactic tides nor stellar encounters could transform a thermal ($\alpha = 1$) or sub-thermal ($\alpha < 1$) to the observed distribution, concluding that dynamical effects cannot drive the binaries away from thermal equilibrium, hence they must already form with a super-thermal distribution. Whether their results withstand a direct N -body integration can be tested with our formalism.

ACKNOWLEDGMENTS

We thank Fabio Antonini, Stephen Justham, Re'em Sari, Hans-Thomas Janka, Kareem El-Badry, Chris Hamilton, Rainer Spurzem, Aleksandra Olejak, and Evgeni Grishin for useful input and discussions. TW acknowledges support from NASA ATP grant 80NSSC24K0768. L.Z. acknowledges support from ERC Starting Grant No. 121817–BlackHoleMergs.

SOFTWARE AND THIRD PARTY DATA
REPOSITORY CITATIONS

Facilities: Max Planck Computing and Data Facility (MPCDF)

Software: MSTAR (Rantala et al. 2020; Mannerkoski et al. 2023), gala (Price-Whelan 2017), cogsworth (Wagg et al. in prep.), COMPAS (Riley et al. 2022)

REFERENCES

- Abbott, R., Abbott, T. D., Acernese, F., et al. 2023, Physical Review X, 13, 011048, doi: [10.1103/PhysRevX.13.011048](https://doi.org/10.1103/PhysRevX.13.011048)
- Andrews, J. J., Chanamé, J., & Agüeros, M. A. 2017, MNRAS, 472, 675, doi: [10.1093/mnras/stx2000](https://doi.org/10.1093/mnras/stx2000)
- Antognini, J. M. O. 2015, MNRAS, 452, 3610, doi: [10.1093/mnras/stv1552](https://doi.org/10.1093/mnras/stv1552)
- Antonini, F., Murray, N., & Mikkola, S. 2014, ApJ, 781, 45, doi: [10.1088/0004-637X/781/1/45](https://doi.org/10.1088/0004-637X/781/1/45)
- Antonini, F., Toonen, S., & Hamers, A. S. 2017, ApJ, 841, 77, doi: [10.3847/1538-4357/aa6f5e](https://doi.org/10.3847/1538-4357/aa6f5e)
- Antonov, V. A., & Latyshev, I. N. 1972, Soviet Ast., 15, 676
- Banik, I., Pittordis, C., Sutherland, W., et al. 2023, MNRAS, doi: [10.1093/mnras/stad3393](https://doi.org/10.1093/mnras/stad3393)
- Bavera, S. S., Fragos, T., Zevin, M., et al. 2021, A&A, 647, A153, doi: [10.1051/0004-6361/202039804](https://doi.org/10.1051/0004-6361/202039804)
- Belczynski, K., Repetto, S., Holz, D. E., et al. 2016, The Astrophysical Journal, 819, 108, doi: [10.3847/0004-637X/819/2/108](https://doi.org/10.3847/0004-637X/819/2/108)
- Binney, J., & Tremaine, S. 2008, Galactic Dynamics: Second Edition (Princeton University Press)
- Björklund, R., Sundqvist, J. O., Puls, J., & Najarro, F. 2021, A&A, 648, A36, doi: [10.1051/0004-6361/202038384](https://doi.org/10.1051/0004-6361/202038384)
- Bovy, J., Leung, H. W., Hunt, J. A. S., et al. 2019, MNRAS, 490, 4740, doi: [10.1093/mnras/stz2891](https://doi.org/10.1093/mnras/stz2891)
- Bovy, J., Rix, H.-W., Schlafly, E. F., et al. 2016, ApJ, 823, 30, doi: [10.3847/0004-637X/823/1/30](https://doi.org/10.3847/0004-637X/823/1/30)
- Bub, M. W., & Petrovich, C. 2020, ApJ, 894, 15, doi: [10.3847/1538-4357/ab8461](https://doi.org/10.3847/1538-4357/ab8461)
- Bulirsch, R., & Stoer, J. 1966, Numerische Mathematik, 8, 1
- Burdge, K. B., El-Badry, K., Kara, E., et al. 2024, The black hole low mass X-ray binary V404 Cygni is part of a wide hierarchical triple, and formed without a kick. <https://arxiv.org/abs/2404.03719>
- Burrows, A., Wang, T., Vartanyan, D., & Coleman, M. S. B. 2024, ApJ, 963, 63, doi: [10.3847/1538-4357/ad2353](https://doi.org/10.3847/1538-4357/ad2353)
- Chebotaev, G. A. 1966, Soviet Ast., 10, 341
- Collins, B. F., & Sari, R. 2008, AJ, 136, 2552, doi: [10.1088/0004-6256/136/6/2552](https://doi.org/10.1088/0004-6256/136/6/2552)
- Correa-Otto, J. A., Calandra, M. F., & Gil-Hutton, R. A. 2017, A&A, 600, A59, doi: [10.1051/0004-6361/201629679](https://doi.org/10.1051/0004-6361/201629679)
- Correa-Otto, J. A., & Gil-Hutton, R. A. 2017, A&A, 608, A116, doi: [10.1051/0004-6361/201731229](https://doi.org/10.1051/0004-6361/201731229)
- Darragh-Ford, E., Hunt, J. A. S., Price-Whelan, A. M., & Johnston, K. V. 2023, ApJ, 955, 74, doi: [10.3847/1538-4357/acf1fc](https://doi.org/10.3847/1538-4357/acf1fc)
- Davis, M., Hut, P., & Muller, R. A. 1984, Nature, 308, 715, doi: [10.1038/308715a0](https://doi.org/10.1038/308715a0)
- de Mink, S. E., & Mandel, I. 2016, MNRAS, 460, 3545, doi: [10.1093/mnras/stw1219](https://doi.org/10.1093/mnras/stw1219)
- du Buisson, L., Marchant, P., Podsiadlowski, P., et al. 2020, MNRAS, 499, 5941, doi: [10.1093/mnras/staa3225](https://doi.org/10.1093/mnras/staa3225)
- Eggleton, P. P. 1983, ApJ, 268, 368, doi: [10.1086/160960](https://doi.org/10.1086/160960)
- Eilers, A.-C., Hogg, D. W., Rix, H.-W., & Ness, M. K. 2019, ApJ, 871, 120, doi: [10.3847/1538-4357/aaf648](https://doi.org/10.3847/1538-4357/aaf648)
- El-Badry, K. 2024, arXiv e-prints, arXiv:2403.12146, doi: [10.48550/arXiv.2403.12146](https://doi.org/10.48550/arXiv.2403.12146)
- El-Badry, K., & Rix, H.-W. 2018, MNRAS, 480, 4884, doi: [10.1093/mnras/sty2186](https://doi.org/10.1093/mnras/sty2186)
- El-Badry, K., Rix, H.-W., & Heintz, T. M. 2021, Monthly Notices of the Royal Astronomical Society, 506, 2269, doi: [10.1093/mnras/stab323](https://doi.org/10.1093/mnras/stab323)
- Eldridge, J. J., & Maund, J. R. 2016, MNRAS, 461, L117, doi: [10.1093/mnrasl/slw099](https://doi.org/10.1093/mnrasl/slw099)
- Flynn, C., Holmberg, J., Portinari, L., Fuchs, B., & Jahreiß, H. 2006, MNRAS, 372, 1149, doi: [10.1111/j.1365-2966.2006.10911.x](https://doi.org/10.1111/j.1365-2966.2006.10911.x)
- Frankel, N., Rix, H.-W., Ting, Y.-S., Ness, M., & Hogg, D. W. 2018, ApJ, 865, 96, doi: [10.3847/1538-4357/aadba5](https://doi.org/10.3847/1538-4357/aadba5)
- Fryer, C. L., Belczynski, K., Wiktorowicz, G., et al. 2012, ApJ, 749, 91, doi: [10.1088/0004-637X/749/1/91](https://doi.org/10.1088/0004-637X/749/1/91)
- Gaia Collaboration, Smart, R. L., Sarro, L. M., et al. 2021, A&A, 649, A6, doi: [10.1051/0004-6361/202039498](https://doi.org/10.1051/0004-6361/202039498)
- Gallegos-Garcia, M., Berry, C. P. L., Marchant, P., & Kalogera, V. 2021, ApJ, 922, 110, doi: [10.3847/1538-4357/ac2610](https://doi.org/10.3847/1538-4357/ac2610)
- Gragg, W. B. 1965, SIAM Journal on Numerical Analysis, 2, 384, doi: [10.1137/0702030](https://doi.org/10.1137/0702030)
- Grishin, E., & Perets, H. B. 2022, MNRAS, 512, 4993, doi: [10.1093/mnras/stac706](https://doi.org/10.1093/mnras/stac706)
- Grishin, E., Perets, H. B., & Fragione, G. 2018, MNRAS, 481, 4907, doi: [10.1093/mnras/sty2477](https://doi.org/10.1093/mnras/sty2477)
- Hamers, A. S., & Lai, D. 2017, MNRAS, 470, 1657, doi: [10.1093/mnras/stx1319](https://doi.org/10.1093/mnras/stx1319)

- Hamers, A. S., Rantala, A., Neunteufel, P., Preece, H., & Vynatheya, P. 2021, *MNRAS*, 502, 4479, doi: [10.1093/mnras/stab287](https://doi.org/10.1093/mnras/stab287)
- Hamers, A. S., & Tremaine, S. 2017, *AJ*, 154, 272, doi: [10.3847/1538-3881/aa9926](https://doi.org/10.3847/1538-3881/aa9926)
- Hamilton, C., & Modak, S. 2023, arXiv e-prints, arXiv:2311.04352, doi: [10.48550/arXiv.2311.04352](https://doi.org/10.48550/arXiv.2311.04352)
- Hamilton, C., & Rafikov, R. R. 2019a, *MNRAS*, 488, 5489, doi: [10.1093/mnras/stz1730](https://doi.org/10.1093/mnras/stz1730)
- . 2019b, *MNRAS*, 488, 5512, doi: [10.1093/mnras/stz2026](https://doi.org/10.1093/mnras/stz2026)
- . 2019c, *ApJL*, 881, L13, doi: [10.3847/2041-8213/ab3468](https://doi.org/10.3847/2041-8213/ab3468)
- . 2021, *MNRAS*, 505, 4151, doi: [10.1093/mnras/stab1284](https://doi.org/10.1093/mnras/stab1284)
- . 2024, *ApJ*, 961, 237, doi: [10.3847/1538-4357/ad0be2](https://doi.org/10.3847/1538-4357/ad0be2)
- Hartman, Z. D., & Lépine, S. 2020, *ApJS*, 247, 66, doi: [10.3847/1538-4365/ab79a6](https://doi.org/10.3847/1538-4365/ab79a6)
- Heger, A., Fryer, C. L., Woosley, S. E., Langer, N., & Hartmann, D. H. 2003, *ApJ*, 591, 288, doi: [10.1086/375341](https://doi.org/10.1086/375341)
- Heisler, J., & Tremaine, S. 1986, *Icarus*, 65, 13, doi: [10.1016/0019-1035\(86\)90060-6](https://doi.org/10.1016/0019-1035(86)90060-6)
- Hellström, C., & Mikkola, S. 2010, *Celestial Mechanics and Dynamical Astronomy*, 106, 143, doi: [10.1007/s10569-009-9248-8](https://doi.org/10.1007/s10569-009-9248-8)
- Henon, M. 1972, *A&A*, 19, 488
- Hernquist, L. 1990, *ApJ*, 356, 359, doi: [10.1086/168845](https://doi.org/10.1086/168845)
- Hobbs, G., Lorimer, D. R., Lyne, A. G., & Kramer, M. 2005, *MNRAS*, 360, 974, doi: [10.1111/j.1365-2966.2005.09087.x](https://doi.org/10.1111/j.1365-2966.2005.09087.x)
- Hut, P. 1981, *A&A*, 99, 126
- . 1984, *Nature*, 311, 638, doi: [10.1038/311638a0](https://doi.org/10.1038/311638a0)
- Hwang, H.-C., Ting, Y.-S., Schlaufman, K. C., Zakamska, N. L., & Wyse, R. F. G. 2021, *MNRAS*, 501, 4329, doi: [10.1093/mnras/staa3854](https://doi.org/10.1093/mnras/staa3854)
- Hwang, H.-C., Ting, Y.-S., & Zakamska, N. L. 2022, *Monthly Notices of the Royal Astronomical Society*, 512, 3383, doi: [10.1093/mnras/stac675](https://doi.org/10.1093/mnras/stac675)
- Inayoshi, K., Hirai, R., Kinugawa, T., & Hotokezaka, K. 2017, *MNRAS*, 468, 5020, doi: [10.1093/mnras/stx757](https://doi.org/10.1093/mnras/stx757)
- Janka, H. T., & Kresse, D. 2024, arXiv e-prints, arXiv:2401.13817, doi: [10.48550/arXiv.2401.13817](https://doi.org/10.48550/arXiv.2401.13817)
- Jiang, Y.-F., & Tremaine, S. 2010, *MNRAS*, 401, 977, doi: [10.1111/j.1365-2966.2009.15744.x](https://doi.org/10.1111/j.1365-2966.2009.15744.x)
- Jiménez-Esteban, F. M., Solano, E., & Rodrigo, C. 2019, *AJ*, 157, 78, doi: [10.3847/1538-3881/aafacc](https://doi.org/10.3847/1538-3881/aafacc)
- Kaib, N. A., & Raymond, S. N. 2014, *ApJ*, 782, 60, doi: [10.1088/0004-637X/782/2/60](https://doi.org/10.1088/0004-637X/782/2/60)
- Kaib, N. A., Raymond, S. N., & Duncan, M. 2013, *Nature*, 493, 381, doi: [10.1038/nature11780](https://doi.org/10.1038/nature11780)
- Karambelkar, V. R., Kasliwal, M. M., Blagorodnova, N., et al. 2023, *ApJ*, 948, 137, doi: [10.3847/1538-4357/acc2b9](https://doi.org/10.3847/1538-4357/acc2b9)
- Katz, B., & Dong, S. 2012, arXiv e-prints, arXiv:1211.4584, doi: [10.48550/arXiv.1211.4584](https://doi.org/10.48550/arXiv.1211.4584)
- Kopparapu, R. K., Hanna, C., Kalogera, V., et al. 2008, *ApJ*, 675, 1459, doi: [10.1086/527348](https://doi.org/10.1086/527348)
- Kouwenhoven, M. B. N., Goodwin, S. P., Parker, R. J., et al. 2010, *MNRAS*, 404, 1835, doi: [10.1111/j.1365-2966.2010.16399.x](https://doi.org/10.1111/j.1365-2966.2010.16399.x)
- Kroupa, P. 2001, *MNRAS*, 322, 231, doi: [10.1046/j.1365-8711.2001.04022.x](https://doi.org/10.1046/j.1365-8711.2001.04022.x)
- Kushnir, D., Katz, B., Dong, S., Livne, E., & Fernández, R. 2013, *ApJL*, 778, L37, doi: [10.1088/2041-8205/778/2/L37](https://doi.org/10.1088/2041-8205/778/2/L37)
- Lee, H. M., & Ostriker, J. P. 1986, *ApJ*, 310, 176, doi: [10.1086/164674](https://doi.org/10.1086/164674)
- Lipunov, V. M., Kornilov, V., Gorbovskoy, E., et al. 2017, *NewA*, 51, 122, doi: [10.1016/j.newast.2016.08.017](https://doi.org/10.1016/j.newast.2016.08.017)
- Liu, B., & Lai, D. 2019, *MNRAS*, 483, 4060, doi: [10.1093/mnras/sty3432](https://doi.org/10.1093/mnras/sty3432)
- Liu, B., Muñoz, D. J., & Lai, D. 2015, *MNRAS*, 447, 747, doi: [10.1093/mnras/stu2396](https://doi.org/10.1093/mnras/stu2396)
- Luhman, K. L. 2014, *ApJ*, 781, 4, doi: [10.1088/0004-637X/781/1/4](https://doi.org/10.1088/0004-637X/781/1/4)
- Luo, L., Katz, B., & Dong, S. 2016, *MNRAS*, 458, 3060, doi: [10.1093/mnras/stw475](https://doi.org/10.1093/mnras/stw475)
- Madau, P., & Dickinson, M. 2014, *ARA&A*, 52, 415, doi: [10.1146/annurev-astro-081811-125615](https://doi.org/10.1146/annurev-astro-081811-125615)
- Mandel, I. 2016, *MNRAS*, 456, 578, doi: [10.1093/mnras/stv2733](https://doi.org/10.1093/mnras/stv2733)
- Mandel, I., & de Mink, S. E. 2016, *MNRAS*, 458, 2634, doi: [10.1093/mnras/stw379](https://doi.org/10.1093/mnras/stw379)
- Mannerkoski, M., Rawlings, A., Johansson, P. H., et al. 2023, *MNRAS*, 524, 4062, doi: [10.1093/mnras/stad2139](https://doi.org/10.1093/mnras/stad2139)
- Marchant, P., Langer, N., Podsiadlowski, P., Tauris, T. M., & Moriya, T. J. 2016, *A&A*, 588, A50, doi: [10.1051/0004-6361/201628133](https://doi.org/10.1051/0004-6361/201628133)
- Marchant, P., Pappas, K. M. W., Gallegos-Garcia, M., et al. 2021, *A&A*, 650, A107, doi: [10.1051/0004-6361/202039992](https://doi.org/10.1051/0004-6361/202039992)
- Matese, J. J., & Whitmire, D. P. 2011, *Icarus*, 211, 926, doi: [10.1016/j.icarus.2010.11.009](https://doi.org/10.1016/j.icarus.2010.11.009)
- McMillan, P. J. 2011, *MNRAS*, 414, 2446, doi: [10.1111/j.1365-2966.2011.18564.x](https://doi.org/10.1111/j.1365-2966.2011.18564.x)
- Melott, A. L., & Bambach, R. K. 2010, *MNRAS*, 407, L99, doi: [10.1111/j.1745-3933.2010.00913.x](https://doi.org/10.1111/j.1745-3933.2010.00913.x)
- Merritt, D. 2013, *Dynamics and Evolution of Galactic Nuclei* (Princeton University Press)
- Michaely, E., & Perets, H. B. 2019, *ApJL*, 887, L36, doi: [10.3847/2041-8213/ab5b9b](https://doi.org/10.3847/2041-8213/ab5b9b)
- . 2020, *MNRAS*, 498, 4924, doi: [10.1093/mnras/staa2720](https://doi.org/10.1093/mnras/staa2720)
- Mikkola, S., & Merritt, D. 2008, *AJ*, 135, 2398, doi: [10.1088/0004-6256/135/6/2398](https://doi.org/10.1088/0004-6256/135/6/2398)

- Mikkola, S., & Tanikawa, K. 1999, MNRAS, 310, 745, doi: [10.1046/j.1365-8711.1999.02982.x](https://doi.org/10.1046/j.1365-8711.1999.02982.x)
- Miyamoto, M., & Nagai, R. 1975, PASJ, 27, 533
- Modak, S., & Hamilton, C. 2023, MNRAS, 524, 3102, doi: [10.1093/mnras/stad2073](https://doi.org/10.1093/mnras/stad2073)
- Moe, M., & Di Stefano, R. 2017, ApJS, 230, 15, doi: [10.3847/1538-4365/aa6fb6](https://doi.org/10.3847/1538-4365/aa6fb6)
- Monroy-Rodríguez, M. A., & Allen, C. 2014, ApJ, 790, 159, doi: [10.1088/0004-637X/790/2/159](https://doi.org/10.1088/0004-637X/790/2/159)
- Mora, T., & Will, C. M. 2004, PhRvD, 69, 104021, doi: [10.1103/PhysRevD.69.104021](https://doi.org/10.1103/PhysRevD.69.104021)
- Naoz, S. 2016, ARA&A, 54, 441, doi: [10.1146/annurev-astro-081915-023315](https://doi.org/10.1146/annurev-astro-081915-023315)
- Naoz, S., Farr, W. M., Lithwick, Y., Rasio, F. A., & Teyssandier, J. 2013, MNRAS, 431, 2155, doi: [10.1093/mnras/stt302](https://doi.org/10.1093/mnras/stt302)
- Navarro, J. F., Frenk, C. S., & White, S. D. M. 1996, ApJ, 462, 563, doi: [10.1086/177173](https://doi.org/10.1086/177173)
- Neijssel, C. J., Vigna-Gómez, A., Stevenson, S., et al. 2019, MNRAS, 490, 3740, doi: [10.1093/mnras/stz2840](https://doi.org/10.1093/mnras/stz2840)
- Oelkers, R. J., Stassun, K. G., & Dhital, S. 2017, AJ, 153, 259, doi: [10.3847/1538-3881/aa6d55](https://doi.org/10.3847/1538-3881/aa6d55)
- Offner, S. S. R., Moe, M., Kratter, K. M., et al. 2023, in Astronomical Society of the Pacific Conference Series, Vol. 534, Protostars and Planets VII, ed. S. Inutsuka, Y. Aikawa, T. Muto, K. Tomida, & M. Tamura, 275, doi: [10.48550/arXiv.2203.10066](https://doi.org/10.48550/arXiv.2203.10066)
- Olejak, A., Belczynski, K., Bulik, T., & Sobolewska, M. 2020, A&A, 638, A94, doi: [10.1051/0004-6361/201936557](https://doi.org/10.1051/0004-6361/201936557)
- Olejak, A., Belczynski, K., & Ivanova, N. 2021, A&A, 651, A100, doi: [10.1051/0004-6361/202140520](https://doi.org/10.1051/0004-6361/202140520)
- Peñarrubia, J., Ludlow, A. D., Chanamé, J., & Walker, M. G. 2016, MNRAS, 461, L72, doi: [10.1093/mnrasl/slw090](https://doi.org/10.1093/mnrasl/slw090)
- Petrovich, C., & Antonini, F. 2017, ApJ, 846, 146, doi: [10.3847/1538-4357/aa8628](https://doi.org/10.3847/1538-4357/aa8628)
- Pittordis, C., & Sutherland, W. 2019, MNRAS, 488, 4740, doi: [10.1093/mnras/stz1898](https://doi.org/10.1093/mnras/stz1898)
- Postnov, K. A., & Yungelson, L. R. 2014, Living Reviews in Relativity, 17, 3, doi: [10.12942/lrr-2014-3](https://doi.org/10.12942/lrr-2014-3)
- Press, W. H., & Teukolsky, S. A. 1977, ApJ, 213, 183, doi: [10.1086/155143](https://doi.org/10.1086/155143)
- Preto, M., & Tremaine, S. 1999, AJ, 118, 2532, doi: [10.1086/301102](https://doi.org/10.1086/301102)
- Price-Whelan, A., Wagg, T., Sipőcz, B., et al. 2024, adrn/gala: v1.8.1, v1.8.1, Zenodo, doi: [10.5281/zenodo.593786](https://doi.org/10.5281/zenodo.593786)
- Price-Whelan, A. M. 2017, The Journal of Open Source Software, 2, doi: [10.21105/joss.00388](https://doi.org/10.21105/joss.00388)
- Quinn, D. P., Wilkinson, M. I., Irwin, M. J., et al. 2009, MNRAS, 396, L11, doi: [10.1111/j.1745-3933.2009.00652.x](https://doi.org/10.1111/j.1745-3933.2009.00652.x)
- Rantala, A., Pihajoki, P., Johansson, P. H., et al. 2017, ApJ, 840, 53, doi: [10.3847/1538-4357/aa6d65](https://doi.org/10.3847/1538-4357/aa6d65)
- Rantala, A., Pihajoki, P., Mannerkoski, M., Johansson, P. H., & Naab, T. 2020, MNRAS, 492, 4131, doi: [10.1093/mnras/staa084](https://doi.org/10.1093/mnras/staa084)
- Rasskazov, A., & Rafikov, R. R. 2023, arXiv e-prints, arXiv:2310.15374, doi: [10.48550/arXiv.2310.15374](https://doi.org/10.48550/arXiv.2310.15374)
- Raveh, Y., Michaely, E., & Perets, H. B. 2022, MNRAS, 514, 4246, doi: [10.1093/mnras/stac1605](https://doi.org/10.1093/mnras/stac1605)
- Riley, J., Mandel, I., Marchant, P., et al. 2021, MNRAS, 505, 663, doi: [10.1093/mnras/stab1291](https://doi.org/10.1093/mnras/stab1291)
- Riley, J., Agrawal, P., Barrett, J. W., et al. 2022, ApJS, 258, 34, doi: [10.3847/1538-4365/ac416c](https://doi.org/10.3847/1538-4365/ac416c)
- Rodriguez, C. L., & Antonini, F. 2018, ApJ, 863, 7, doi: [10.3847/1538-4357/aace4](https://doi.org/10.3847/1538-4357/aace4)
- Ruiter, A. J., Belczynski, K., Sim, S. A., et al. 2011, MNRAS, 417, 408, doi: [10.1111/j.1365-2966.2011.19276.x](https://doi.org/10.1111/j.1365-2966.2011.19276.x)
- Samsing, J., MacLeod, M., & Ramirez-Ruiz, E. 2014, ApJ, 784, 71, doi: [10.1088/0004-637X/784/1/71](https://doi.org/10.1088/0004-637X/784/1/71)
- Sana, H., de Mink, S. E., de Koter, A., et al. 2012, Science, 337, 444, doi: [10.1126/science.1223344](https://doi.org/10.1126/science.1223344)
- Schwarzschild, K. 1916, Abh. Konigl. Preuss. Akad. Wissenschaften Jahre 1906,92, Berlin,1907, 1916, 189
- Shenar, T., Sana, H., Mahy, L., et al. 2022, Nature Astronomy, 6, 1085, doi: [10.1038/s41550-022-01730-y](https://doi.org/10.1038/s41550-022-01730-y)
- Smith, R., Flynn, C., Candlish, G. N., Fellhauer, M., & Gibson, B. K. 2015, MNRAS, 448, 2934, doi: [10.1093/mnras/stv228](https://doi.org/10.1093/mnras/stv228)
- Stegmann, J., Antonini, F., & Moe, M. 2022a, MNRAS, 516, 1406, doi: [10.1093/mnras/stac2192](https://doi.org/10.1093/mnras/stac2192)
- Stegmann, J., Antonini, F., Schneider, F. R. N., Tiwari, V., & Chattopadhyay, D. 2022b, PhRvD, 106, 023014, doi: [10.1103/PhysRevD.106.023014](https://doi.org/10.1103/PhysRevD.106.023014)
- Tauris, T. M., & van den Heuvel, E. P. J. 2023, Physics of Binary Star Evolution. From Stars to X-ray Binaries and Gravitational Wave Sources, doi: [10.48550/arXiv.2305.09388](https://doi.org/10.48550/arXiv.2305.09388)
- Tian, H.-J., El-Badry, K., Rix, H.-W., & Gould, A. 2020, ApJS, 246, 4, doi: [10.3847/1538-4365/ab54c4](https://doi.org/10.3847/1538-4365/ab54c4)
- Tokovinin, A. 2020, Monthly Notices of the Royal Astronomical Society, 496, 987, doi: [10.1093/mnras/staa1639](https://doi.org/10.1093/mnras/staa1639)
- Toonen, S., Perets, H. B., & Hamers, A. S. 2018, A&A, 610, A22, doi: [10.1051/0004-6361/201731874](https://doi.org/10.1051/0004-6361/201731874)
- Toonen, S., Portegies Zwart, S., Hamers, A. S., & Bandopadhyay, D. 2020, A&A, 640, A16, doi: [10.1051/0004-6361/201936835](https://doi.org/10.1051/0004-6361/201936835)

- Toy, M., Wiseman, P., Sullivan, M., et al. 2023, MNRAS, 526, 5292, doi: [10.1093/mnras/stad2982](https://doi.org/10.1093/mnras/stad2982)
- Trani, A. A., & Spera, M. 2023, in *The Predictive Power of Computational Astrophysics as a Discover Tool*, ed. D. Bisikalo, D. Wiebe, & C. Boily, Vol. 362 (Cambridge University Press), 404–409, doi: [10.1017/S1743921322001818](https://doi.org/10.1017/S1743921322001818)
- van den Heuvel, E. P. J., Portegies Zwart, S. F., & de Mink, S. E. 2017, MNRAS, 471, 4256, doi: [10.1093/mnras/stx1430](https://doi.org/10.1093/mnras/stx1430)
- van Son, L. A. C., de Mink, S. E., Renzo, M., et al. 2022, ApJ, 940, 184, doi: [10.3847/1538-4357/ac9b0a](https://doi.org/10.3847/1538-4357/ac9b0a)
- Vigna-Gómez, A., Willcox, R., Tamborra, I., et al. 2023, arXiv e-prints, arXiv:2310.01509, doi: [10.48550/arXiv.2310.01509](https://doi.org/10.48550/arXiv.2310.01509)
- Vink, J. S., de Koter, A., & Lamers, H. J. G. L. M. 2001, A&A, 369, 574, doi: [10.1051/0004-6361:20010127](https://doi.org/10.1051/0004-6361:20010127)
- Wagg, T., Broekgaarden, F. S., de Mink, S. E., et al. 2022, ApJ, 937, 118, doi: [10.3847/1538-4357/ac8675](https://doi.org/10.3847/1538-4357/ac8675)
- Weinberg, M. D., Shapiro, S. L., & Wasserman, I. 1987, ApJ, 312, 367, doi: [10.1086/164883](https://doi.org/10.1086/164883)
- Wen, L. 2003, ApJ, 598, 419, doi: [10.1086/378794](https://doi.org/10.1086/378794)
- Whitmire, D. P., & Jackson, A. A. 1984, Nature, 308, 713, doi: [10.1038/308713a0](https://doi.org/10.1038/308713a0)
- Yoo, J., Chanamé, J., & Gould, A. 2004, ApJ, 601, 311, doi: [10.1086/380562](https://doi.org/10.1086/380562)
- Zahn, J. P. 1975, A&A, 41, 329